

Paleoceanography and Paleoclimatology®

RESEARCH ARTICLE

10.1029/2021PA004404

Key Points:

- A comparison of three methods to determine ice rafted debris (IRD) abundances in Antarctic sediment cores was undertaken
- X-radiograph (>2 mm), sieve (250 µm–2 mm), and laser (125 µm–2 mm) based methods produced comparable results, but with notable differences
- All approaches have caveats and require independent lines of evidence to rule out deposition by other processes

Correspondence to:

R. McKay,
robert.mckay@vuw.ac.nz

Citation:

McKay, R., Albot, O., Dunbar, G. B., Lee, J. I., Lee, M. K., Yoo, K.-C., et al. (2022). A comparison of methods for identifying and quantifying ice rafted debris on the Antarctic margin. *Paleoceanography and Paleoclimatology*, 37, e2021PA004404. <https://doi.org/10.1029/2021PA004404>

Received 6 JUN 2020
Accepted 8 MAR 2022

Author Contributions:

Conceptualization: Robert McKay
Data curation: Olga Albot
Formal analysis: Robert McKay, Olga Albot, Gavin B. Dunbar, Jae Il Lee, Min Kyung Lee, Kyu-Cheul Yoo, Sunghan Kim, Nikita Turton, Richard Levy
Funding acquisition: Robert McKay, Jae Il Lee, Min Kyung Lee, Kyu-Cheul Yoo, Sunghan Kim, Richard Levy
Investigation: Robert McKay, Olga Albot, Gavin B. Dunbar, Jae Il Lee, Min Kyung Lee, Kyu-Cheul Yoo, Sunghan Kim, Richard Levy
Methodology: Robert McKay, Olga Albot, Gavin B. Dunbar, Nikita Turton, Denise Kulhanek, Molly Patterson
Project Administration: Robert McKay

© 2022. The Authors.

This is an open access article under the terms of the Creative Commons Attribution License, which permits use, distribution and reproduction in any medium, provided the original work is properly cited.

A Comparison of Methods for Identifying and Quantifying Ice Rafted Debris on the Antarctic Margin

Robert McKay¹ , Olga Albot¹, Gavin B. Dunbar¹ , Jae Il Lee² , Min Kyung Lee², Kyu-Cheul Yoo² , Sunghan Kim², Nikita Turton^{1,3}, Denise Kulhanek⁴, Molly Patterson⁵ , and Richard Levy^{1,3} 

¹Antarctic Research Centre, Victoria University of Wellington, Wellington, New Zealand, ²Korea Polar Research Institute, Incheon, Republic of Korea, ³GNS Science, Lower Hutt, New Zealand, ⁴Institut für Geowissenschaften, Christian-Albrechts-Universität zu Kiel, Kiel, Germany, ⁵Department of Geological Sciences, Binghamton University, State University of New York, Binghamton, NY, USA

Abstract Quantification of ice rafted debris (IRD) abundances in deep-sea records is often used as a key proxy for identifying links between ice sheet instability and the oceanic overturning circulation. There currently exist multiple methods to determine IRD content in deep-sea sediment cores. The preference for a given method is often determined by the accessibility to core material and destructive nature of some methods. While many studies have discussed the caveats between linking IRD to ice sheet dynamics, the uncertainties relating to the methodological approaches are often not considered in the interpretation or comparisons between different IRD datasets, particularly in the Antarctic. To address this, we compare three independent methodologies of obtaining IRD abundances and also discuss how different approaches will affect determinations of mass accumulation rates (MARs). The three methodologies we examine include: counting clasts >2 mm in x-radiographs; the sieved weight percentage of the medium-to-coarse sand fraction (250 µm–2 mm); and volumetric estimates of the >125 µm sand fraction using laser diffraction particle size analysis. The x-radiograph and sieve methods produced comparable results, while the laser particle size analysis, although showing comparable long-term signals at most locations, in general has lower correlation to the other two methods and therefore a higher potential to obtain a noisy signal. We discuss the caveats associated with all methods, and emphasize that a combination of multiple methods should ideally be employed when assessing if a core is suitable for IRD study, and if sand or gravel fractions are accurately reflecting contents of IRD.

Plain Language Summary Ice rafted debris (IRD) records in the deep sea are fundamental indicators of past ice sheet change. However, using different methods to quantify IRD abundance in the Antarctic has the potential to produce conflicting results. We assess the role that methodological approaches may account for such differences, through a comparison of three commonly used methods.

1. Introduction

Records of the flux of ice rafted debris (IRD) to the seafloor over time have provided fundamental insights into the past behavior of marine-terminating polar ice sheets. Debate about the exact relationship between IRD content of seafloor sediment and ice sheet dynamics is ongoing. Several reasons for this debate exist. First, studies are highly variable in defining the size fraction that is used for determining IRD and measuring it (Andrews, 2000; Conolly & Ewing, 1965; Diekmann et al., 2003; Passchier, 2011; Patterson et al., 2014; Ruddiman, 1977), potentially leading to different results from different researchers. Second, IRD could conceivably reflect (a) a change in the flux of icebergs across the study site, (b) a change in the mass of debris carried by icebergs, (c) a change in the melt rate of icebergs across the study site, or (d) some combination of all three (Cook et al., 2014; Hillenbrand et al., 2009; Starr et al., 2021; Williams et al., 2010). Despite these caveats, it is clear from geological archives that IRD commonly displays a coherent relationship with other proxies indicating that underlying climatic drivers explain many IRD records. There have recently been a large number of studies reconstructing IRD abundance (e.g., Hillenbrand et al., 2009; Kanfoush et al., 2002, 2000; Ó Cofaigh et al., 2001) or IRD flux in the Southern Ocean and Antarctic margin (Carter et al., 2002; Diekmann, 2007; Diekmann et al., 2003; Grobe & Mackensen, 1992; Hillenbrand et al., 2002; Ó Cofaigh et al., 2001; Passchier, 2011; Patterson et al., 2014; Starr et al., 2021; Weber et al., 2014). It is important to note that many IRD studies commonly utilize different methods for measuring its abundance in the sediment matrix. All of these methods quantify the measurement of

Resources: Olga Albot, Jae Il Lee, Min Kyung Lee, Kyu-Cheul Yoo, Sunghan Kim, Nikita Turton, Denise Kulhanek

Software: Robert McKay

Supervision: Robert McKay

Validation: Robert McKay, Min Kyung Lee

Writing – original draft: Robert McKay, Olga Albot

Writing – review & editing: Robert McKay, Olga Albot, Gavin B. Dunbar, Jae Il Lee, Min Kyung Lee, Kyu-Cheul Yoo, Sunghan Kim, Nikita Turton, Denise Kulhanek, Molly Patterson, Richard Levy

coarse grain sizes (with various size fraction cut offs) that provide a proxy measure for the total IRD content in a sample, which in reality comprises all grain sizes, but it is difficult to isolate the IRD fraction at finer grain sizes (e.g., in the mud fraction). However, depending on the depositional setting and processes, some of the coarse size fractions used for IRD proxies may capture grains that are not ice rafted, or lack statistical significance when measuring the abundance of “outsized” grains in a grain size distribution. In this paper, we conduct a comparison of three commonly used methods to determine IRD abundance to assess if different signals in the resultant datasets can be explained by the use of different laboratory approaches.

1.1. Paleoceanographic Significance of IRD

The presence of outsized sand and gravel clasts in deep-sea muds recovered from high latitudes is commonly interpreted to represent the flux of melting icebergs calving off marine-terminating glaciers, and thus reflects changes in the mass balance of ice sheets (Jansen et al., 2000; Kanfoush et al., 2000). The significance of such records was recognized in north Atlantic sediments, where prominent layers of concentrated IRD with a Laurentian provenance, termed Heinrich layers, were identified in sediment cores (Andrews & Voelker, 2018; Bond et al., 1992; Dowdeswell et al., 1999; Heinrich, 1988; Hemming, 2004). The leading hypothesis for the genesis of these layers is that they reflect ice shelf collapses from subsurface oceanic warming, resulting in a surge of the marine margins of the Laurentide Ice Sheet which released large quantities of debris-rich icebergs into the north Atlantic (Flückiger et al., 2006; Hulbe et al., 2004; Li & Piper, 2015; Marcott et al., 2011). Because the Antarctic Ice Sheets (as a total average) lose ~50% of their mass by iceberg calving from outlet glaciers and ice streams (Depoorter et al., 2013), it is proposed IRD records that lie in the primary iceberg pathways on the Antarctic continental margin are a reliable proxy of shifting ice sheet dynamics (Hillenbrand et al., 2009; Passchier, 2011; Patterson et al., 2014; Weber et al., 2014; Williams et al., 2010). However, mass loss by iceberg calving on individual ice shelves can vary between 10% and 90%, with the remainder taken up by basal melt, which could result in regional differences of IRD abundances and the relationship to ice dynamics (Depoorter et al., 2013). Iceberg calving from thinning ice shelves in negative mass balance is also dominated by more frequent calving events, and this process is distinct from the more periodic processes of isolated tabular icebergs that break up from ice shelves in neutral or positive mass balance regimes (Liu et al., 2015). Consequently, it is proposed by many of the above studies that an enhanced signal of IRD should be present in the deep ocean proximal to Antarctica during large deglaciation events.

The frequency characteristics of such IRD pulses from Prydz Bay and the Adélie Land continental margin of Antarctica throughout the Miocene, Pliocene, and Pleistocene are consistent with pacing by changes in Earth’s orbital geometry (i.e., Milankovitch cycles), which suggests that the volume of Antarctica’s ice sheet also fluctuate on this timescale (Escutia et al., 2003; Hansen et al., 2015; Lucchi et al., 2002; Passchier, 2011; Patterson et al., 2014; Williams & Handwerger, 2005; Williams et al., 2010). Millennial-scale pulses of IRD to the Scotia Sea during the last deglaciation (20–9 kyr) are also interpreted to represent episodes of Antarctic marine ice sheet instability on sub-orbital timescales, indicating that IRD peaks and fluxes in this setting represent major deglaciation events and have the potential to provide high-resolution archives of dynamic ice sheet discharge leading into interglacial periods (Diekmann et al., 2003; Ehrmann & Grobe, 1991; Hepp et al., 2006; Hillenbrand & Fütterer, 2001; Weber et al., 2014).

1.2. Physical Controls on IRD Deposition

The interpretation and significance of IRD is likely to vary in different regions, as the debris content of icebergs is determined by numerous factors. Glaciers and ice streams in warmer glacial thermal regimes produce and carry abundant sand and silt-sized grains by means of glacial erosion of primary bedrock (Evans & Pudsey, 2002). However, in West Antarctica, dynamic ice streams override and rework pre-existing muddy tills and glacimarine muds/diamictites that have accumulated in Late Cenozoic sedimentary basins that are several kilometers thick. In this case, sand and gravel eroded directly from bedrock may be relatively less abundant than for sites bordering East Antarctica, although recycling of clasts from older glacial diamictites is likely to occur (McKay et al., 2019; Tulaczyk et al., 1998). Additionally, the base of large ice shelves, such as the Ross Ice Shelf, are commonly debris free, and large iceberg calving events from such ice shelves may deliver little IRD to the ocean (Anderson, 1999).

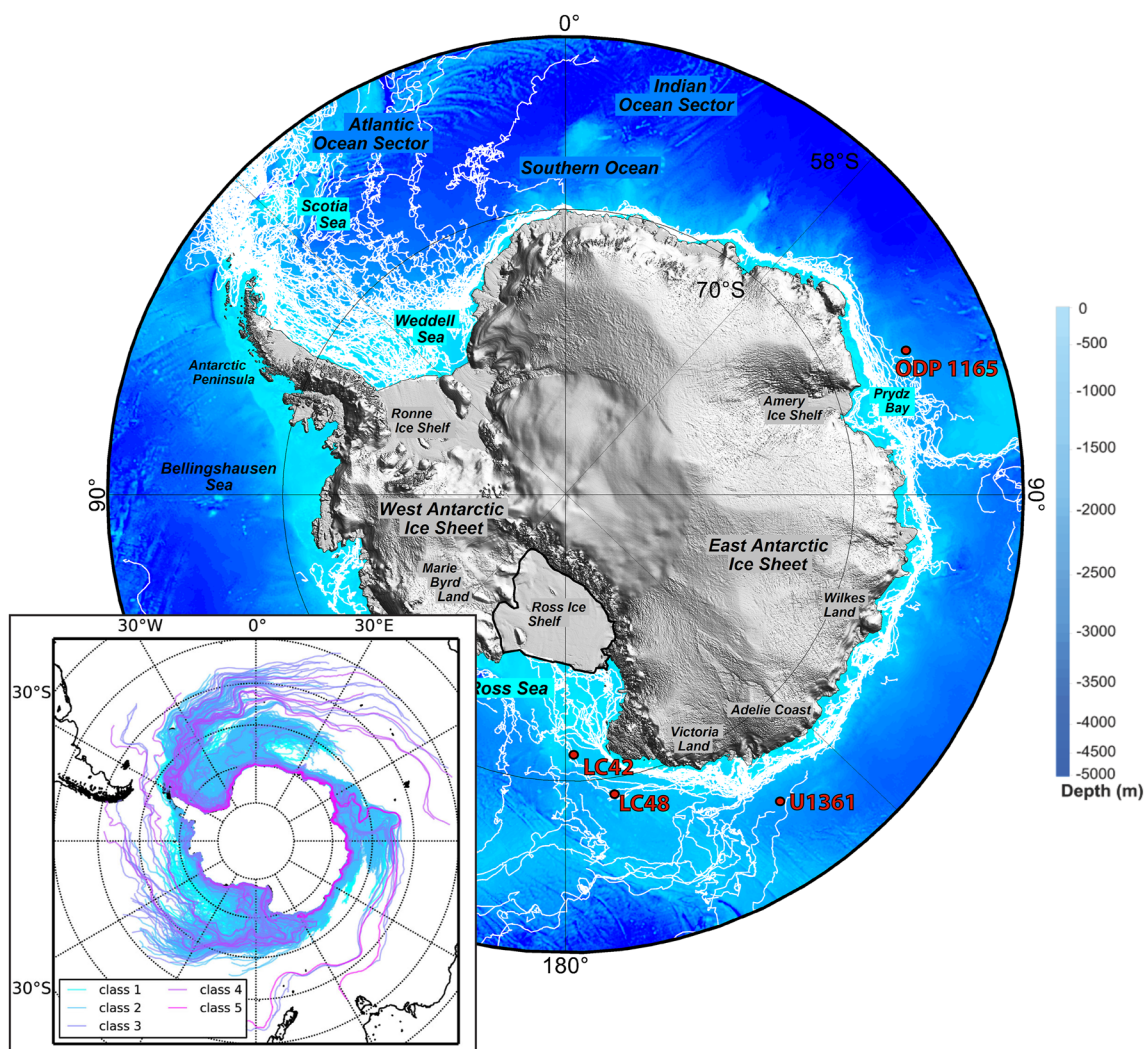


Figure 1. Map of the Antarctic continent and offshore bathymetry showing sites in this study. White lines around the Antarctic continent depict modern iceberg ($>5 \text{ km}^2$) tracks between 1999 and 2009 (Stuart & Long, 2011). Topography and bathymetry derived from theETOPO1 global relief model (Amante & Eakins, 2009). Insert: 12 years simulation of modeled trajectories of small (class 1 = $<1 \text{ km}^2$ surface area) to large (class 5 = $>1,000 \text{ km}^2$ surface area) icebergs (from: Rackow et al., 2017).

Glacier speed and calving rate both further influence iceberg production and size (Bassis et al., 2017), while other controls such as coastal morphology, sea ice extent, sea surface temperatures (SSTs) and current directions exert a strong influence on iceberg survival, residence time, and the spatial distribution of icebergs (Gilbert, 1990; Jansen et al., 2000; Starr et al., 2021; Teitler et al., 2010; Figure 1). In addition, IRD abundance in the depositional record may also reflect regional processes controlled by the ice sheet response to glacial-interglacial environmental variability, such as current winnowing and changes in sedimentation rates, rather than regional-scale episodes of increased/decreased iceberg calving (McCave & Andrews, 2019; Ó Cofaigh & Dowdeswell, 2001).

1.3. Issues With the Interpretation of IRD Records

Given the number of complicated controls on IRD deposition outlined above, there is long standing debate regarding what IRD flux represents in terms of ice sheet stability and the methodology used to derive IRD records. Clark and Pisias (2000) propose that only greatly enhanced fluxes of IRD from the Antarctic ice sheets deposited over a large area can be unambiguously interpreted in terms of changes in dynamic ice sheet discharge. This assertion is dependent on a number of assumptions, including whether or not: (a) IRD is delivered through fallout from icebergs rather than sea ice, because sea-ice transport of IRD in the Antarctic is (at present) restricted

to coastal settings (Chewings et al., 2014); (b) an increase in IRD is representative of an increased iceberg flux as opposed to a greater amount of debris incorporated at the base of the ice sheet from which icebergs are calved off or changes in iceberg melt rates; and (c) the amount of IRD is similar in all icebergs, and thus, whether or not there is a correlation between IRD concentration and iceberg flux (Clark & Pisias, 2000). Consequently, the IRD flux to the seafloor is dependent on the number and size of icebergs passing over the site, the proximity to the calving glaciers, the type and size of the glacier it has calved from, drift paths relating to ocean currents changing through time, and the variability of sea ice and SSTs. All of these factors vary greatly with local climatic, oceanographic and glacial regimes, which can be assessed via comparisons to multiproxy datasets and modeling studies (Cook et al., 2014; Gilbert, 1990; Golledge et al., 2014; Powell & Domack, 2002; Starr et al., 2021).

We do not attempt to address these complex issues regarding the relationship between ice dynamics and IRD flux in this paper, other than to note that site-specific considerations must clearly be accounted for when interpreting and applying a methodology to these records. We also note a multiproxy approach can at least constrain some of the environmental variables thought to control IRD flux, but clearly our understanding would benefit from more comprehensive observations of modern processes.

1.4. Criterion for Defining IRD in Antarctic Margin Sediments

In recent studies of ice proximal environments on the continental rise to abyssal plain in Antarctica, a range of grain sizes have commonly been used to define the IRD fraction including, but not restricted to, 125 µm–2 mm, 250 µm–2 mm, or >2 mm. These ranges are determined on the basis that the settling velocity of such material is too high for it to be transported over long distances by processes other than ice rafting. However, downslope mass transport processes must still be considered for sites proximal to the Antarctic margin (Cowan et al., 2020; Kanfoush et al., 2000; Murphy et al., 2002; Patterson et al., 2014; St. John & Krissek, 1999; Weber et al., 2014). In the Antarctic, transport of sediment by sea ice in coastal regions is generally restricted to the 63–150 µm fraction, that is, a size fraction that can readily be blown on to sea ice by wind, with most sand-size sediment restricted to coastal fast ice <5 km offshore (Chewings et al., 2014). Similarly, resuspension by traction currents is generally restricted to the <63 µm fraction (Andrews, 2000) but could be higher in regions with extreme bottom current speeds (Lamy et al., 2015; McCave & Andrews, 2019). Grain shape and surface texture have been used to identify sediment transport via these different processes, with sub-angular to angular clasts containing a high abundance of fractures and striations/gouges used as indicators of an iceberg-rafted, rather than sea ice-rafted, origin (St. John et al., 2015). However, this alone does not confirm that a grain is rafted by either an iceberg or sea ice to the site, as a glacial erosion signature is likely to be pervasive on the Antarctic continental margin as this is the predominant mechanism for physical weathering of sediment. Similarly, well-rounded grain shapes have been used in some settings to distinguish grains that have been potentially wind-blown onto sea ice and subsequently transported offshore (Passchier et al., 2021). However, such rounding could also be inherited from non-glacial strata that have been eroded and deposited within sub-glacially deposited diamictites. For example, subglacially deposited diamictites in the AND-1B drill core from the Ross Sea continental shelf have clasts contents that comprise up to 15% of rounded quartz with preserved chemical overgrowths derived from the Devonian Beacon Supergroup fluvial deposits, with little alteration of the original grain shape (Talarico et al., 2012). Assessment of volcanic tephra grains in the coarse fraction can help assess if primary ashfall onto the ocean surface, or drifting sea ice can account for delivery of coarse grains into the deep ocean, although distinguishing ice rafted versus primary volcanic ashfall can be difficult in regions dominated by active volcanics (Nielsen et al., 2007). Moreover, re-deposition via any of the above processes is likely to be rapid and include grains where the original subglacial grain shape/surface textures are likely to remain preserved.

2. Methods of Determining IRD Flux

An issue that is often overlooked in interpreting and comparing IRD records is that a number of different methods are employed to categorize and quantify the IRD content in sediment cores (Andrews, 2000). The most frequently used methods in the Antarctic region include: (a) counting particles in the 150 µm–2 mm size fraction under the microscope where particles categorized as IRD are quartz, feldspars, mafic minerals, and metamorphic lithic fragments (Kanfoush et al., 2000; Murphy et al., 2002); (b) measuring the weight percentages of the 250 µm–2 mm size fraction and then visually checking by microscope whether the grains are non-biogenic, volcanic, or diagenetic in origin and correcting for these by numerical or physical removal (Cowan et al., 2008;

Patterson et al., 2014; St. John & Krissek, 1999); (c) visually counting lithogenic particles (either >1 or >2 mm) from the x-radiographs of the sediment core, either by scans on the half/whole cores or subsampled by slabs/u-channels, and binning these into discrete intervals to determine a number of grains per volume of sediment (Cowan et al., 2008; Grobe, 1987; Weber et al., 2014); and (d) Laser Particle Sizer Analysis (LPSA) of the size-frequency distribution and determination of the relative volume percentage of the 125 μm –2 mm fraction (Hansen et al., 2015; Passchier, 2011).

We do not comprehensively cross compare all published methods in this paper and have chosen methods to compare that rely on either a volumetric, weight or counting approach, but similar caveats and issues should be considered and investigated for other methods not examined here. Each of the methods we investigate utilizes one of these approaches, and has previously been applied to sediment cores from the continental margin of the Antarctic, and as noted earlier, inferred through the use of multiproxy approaches to identify changes in ice sheet dynamics.

Although grains of all sizes can be carried by icebergs, the lower size limit of 125 or 250 μm used to identify unambiguous IRD is often assumed to eliminate the finer material transported by sea ice, bottom currents, wind or turbidity/gravity currents. However, the abundance, and spatial and temporal patterns of IRD estimates can vary depending on the grain size fraction being measured, and therefore site-specific considerations are needed (Andrews, 2000). It is even more critical to assess the relevance of these size limits in determining an ice rafted origin for sediment when working on a continental margin, as medium sand and coarser grains can be transported to the deep ocean via density currents or mass flow processes, while high energy currents can act to resuspend sediment. Additionally, diagenetic and biogenic material can also contribute to this size fraction and needs to be accounted for in any calculations of IRD. Comparison of modern drift pathways of large icebergs ($>5 \text{ km}^2$) indicate that in Antarctica, iceberg concentrations are highest over the continental rise region (Figure 1). Even under scenarios of greatly reduced ice sheet volume, the current system responsible for this drift pattern is unlikely to have changed direction or location due to bathymetric and geostrophic considerations (DeConto et al., 2007). All of the sites utilized in this paper lie just to the north of the eastward flowing pathway of the Antarctic Slope Current, from which smaller icebergs are transported northward via eddies and gyres (Rackow et al., 2017; Tournaire et al., 2016). It is argued that because this current and associated eddies and gyres focuses icebergs, it holds the most potential to obtain records of past changes in ice dynamics (Passchier, 2011; Patterson et al., 2014; Weber et al., 2014; Williams et al., 2010), but this depositional setting is also complicated by other continental margin sedimentary processes (Donda et al., 2007; King et al., 2022). Site-specific considerations must therefore be taken into account, via development of a full depositional model using complementary datasets, including seismic survey data, sedimentary facies analysis, and geochemical data.

All methods of determining IRD have advantages and uncertainties (Table 1). For example, LPSA is a rapid and simple method, and has major advantages over other grain size methods, such as SediGraph or coulter counter, in that it can quickly measure the entire frequency distribution of grain size in the mud to sand fraction (0–2 mm). All methods that use samples from sediment cores are limited by the availability of sample, due to the small core diameters, and pressures from other sampling requirements. The consequence of this is that the minimum sample volume/mass required significantly increases with the maximum grain size that is to be captured accurately (Kowalenko & Babuin, 2013; Rawle, 2015). In addition to sample availability, the LPSA method is also limited by the analytical method. First, the sample mass required to obtain obscuration values suitable to accurately measure a given size range greatly varies, with sand-rich samples requiring more sediment than mud-rich sediment. Consequently, in mud-rich sediments that are common in glacial settings the LPSA is often limited to using sample sizes of 0.1–1 g of sediment, but a greater volume of sediment is required to capture the sand fraction more precisely in these systems (\sim 1–2 g for medium sands). This issue led Kowalenko and Babuin (2013) to conclude that laser diffraction methods were not well suited to sample where the entire distribution range from clay to sands needs to be measured precisely. The exact mass of sediment required varies between instruments and the dispersion module, which controls the volume of water and thus the concentration of the sediment circulating in the analyzer. However, a key point here is that the mass of sediment analyzed is controlled by the need to obtain a correct obscuration value on the instrument, rather than sample availability itself.

An additional consideration is that the LPSA measurement is derived from a volume percentage calculation from a small total sample volume, and volume percentage can only be converted to weight via assumptions of grain shape, density and optical properties (Blott & Pye, 2006). Blott and Pye (2006) also note issues with LPSA

Table 1*Summary of IRD Methods Examined in This Study, Alongside Benefits, and Caveats for Each Method as Discussed in the Main Text*

Method	Size range measured	Type of measurement	Comments
Laser Particle Sizer Analysis	125 µm–2 mm	Volume	Analytical restrictions for sample masses ($\sim <1$ g) in mud-rich samples reduces statistical significance of coarse sand fraction. Requires effective dissolution of biogenic opal/carbonate, and other non-IRD components from all size fractions prior to measurement. To determine Mass Accumulation Rates, these components have to be quantified using other estimates. Measures entire size fraction, and frequency distribution curves can be used to assess if >125 µm fraction is distinct from other sediment populations (e.g., well-sorted sands).
Sieve	250 µm–2 mm	Weight	Relatively rapid method, although chemical dissolution methods of entire sediment population can be time consuming. Sample availability from core material is generally 10–20 g (but could be larger if needed), and statistical significance of coarse sand fraction will reduce with sample size.
X-radiograph count	>2 mm	Count	Requires removal of biogenic opal/carbonate, and other non-IRD components from 250 µm to 2 mm fraction prior to weighing. No subsequent corrections are required for the IRD component of the Mass Accumulation Rates calculation. Only measures <250 µm and 250 µm–2 mm fractions, and requires additional frequency distribution analysis (esp., LPSA) to confirm if 250 µm–2 mm fraction is distinct from non-IRD populations. Relatively rapid method. Chemical dissolution/physical removal of biogenic material only required on 250 µm–2 mm fraction (e.g. centrifuging is not required), but requires supporting LPSA and processing time (see above).
			Statistical significance is dependent on concentration/size of IRD in core, and the core diameter. Correction for biogenic opal is not required, as this is generally less than 2 mm, while large biogenic carbonate particles are unlikely to be counted as IRD. Other non-IRD components (ash, diagenetic minerals) could be potentially counted as IRD. No subsequent corrections are required for the IRD component of the Mass Accumulation Rates calculation. Some user-based subjectively in identifying IRD, and size cut-off used is dependent on image quality, grain density, and contrast with background sediment. These will vary from core to core, as well as across facies variations within a core. X-radiograph images can be used to assess for winnowing, or other deposition processes that could account for >2 mm grains in the core.
			Rapid, potentially non-destructive method, but requires consistent training and cross validation between two (or more) users.

software modelling of sand distributions that use assumptions of log-normal distributions. IRD is unlikely to have such a distribution, and is more likely to approximate a uniform distribution, although this is source lithology dependent. Modelling normal distributions is most problematic in highly skewed, truncated or bimodal samples (Blott & Pye, 2006), and such samples are pervasive in glaciated settings.

Given the above issues, a caveat exists as to whether the number of medium-sand and coarser particles present in a sample is a good representation of their actual abundance in sediment in any of the methods we examine. This problem can be illustrated by a simple example of two grains in a measurement having a diameter of 125 and 1,250 μm , using lower end member values for total sample size. The larger of these grains has 1,000 times the volume of the smaller grain. Assuming a density of quartz (2.65 g/cm^3), the 1,250 μm grain has a mass of 0.0027 g, and for a bulk sample weight of 0.15 g used in the LPSA measurement this single grain could represent up to 1.8% of the total. This caveat also exists for sieving methods, as the presence or absence of a few coarse sand grains can therefore make a large difference to the estimated weight percentage of IRD in small bulk samples. In sieving, to obtain 1.8% of this size fraction from 5 g of sediment would require >30 grains of a 1,250 μm diameter, although a single 2 mm grain could represent up to 0.88% in a 5 g sieve sample (and 7.4% in a 0.15 g LPSA sample).

So although the above examples show that both methods do have issues with statistical significance due to sample availability, a key difference is that sieving is not analytically limited to having a prescribed sample size in the same way as the LPSA method, which is dependent on obscuration value for the analysis (Kowalenko & Babuin, 2013). While not completely overcoming these statistical issues (particularly at the upper size limits of 1–2 mm), in most studies a greater sample mass should be measured (10–20 g) in sieving than the example given above. In reality, in all of these methods there would be sand grains of a range of values between 125 μm and 2 mm. These hypothetical scenarios only serve to highlight the relative difference in the statistical significance when measuring sand grains from small sample volumes in LPSA, relative to those of sieving. For example, a single 1062.5 μm grain (midpoint of the LPSA measurement range) would give a 0.18% value in a 0.9 g of LPSA sample (upper mass value measured on the LPSA in this study), whereas in sieving, a 1,125 μm grain (midpoint of sieve method) would be only 0.02% in a 10 g sample, a preferable lower limit of sieving in this study.

The above examples do not downplay that issues with statistical significance in the sieve and x-radiograph counting methods also exist, and limited sample volume is also likely to impact the reproducibility of the abundance of the $>250 \mu\text{m}$ fraction. However, the above scenario highlights uncertainties that are potentially (but not always) an order of magnitude larger using the LPSA method, with the potential that this could create a noisier signal. To assess the relative impact of this, we conduct reproducibility experiments for both the LPSA and sieving methods, as well as the x-radiograph counting method (see Section 3.3).

In addition, all methods require the assessment of whether a grain in the designated IRD size fraction is authigenic, biogenic or volcanic in origin (Table 1). On its own, the LPSA method cannot reliably distinguish between such grains, and therefore this method requires confidence that dissolution of these biogenic components in both the fine and coarse fraction has been successfully conducted prior to analysis (see Section 3), and no diagenetic, volcanic or eolian particles are present. In sieve-based methods, the abundance of authigenic and biogenic material only needs to be removed from the coarse fraction (as IRD MAR and abundance is measured relative to the entire sediment population), and its presence and confirmation of successful removal can be readily assessed by microscope examination. Like the LPSA method, the sieve-based methods may also require independent analysis of the fine grain fraction, or assessment of the core face or x-radiographs to identify sediment facies, to understand the context in which the $>250 \mu\text{m}$ fraction was deposited. That is, to determine whether processes such as gravity flows, wind-blown grains, or winnowing could enhance the abundance of the $>250 \mu\text{m}$ size fraction independent of the flux of IRD.

Visually counting grains on x-radiographs or under the microscope, is potentially subject to operator-induced uncertainties through misidentification of IRD but has considerable advantages over other methods as it can measure the larger-outsized clasts. X-radiographs also have the substantial advantage in that they allow for continuous data to be produced downcore, in contrast to the discrete sampling required for sieve and LPSA methods (Grobe, 1987). It also readily allows for the identification of sedimentary structures that could indicate traction currents and sediment winnowing that would otherwise result in an overestimate of IRD content. Traditionally, the optimal method for creating x-radiograph images involves obtaining 1 cm thick slabs of the sediment

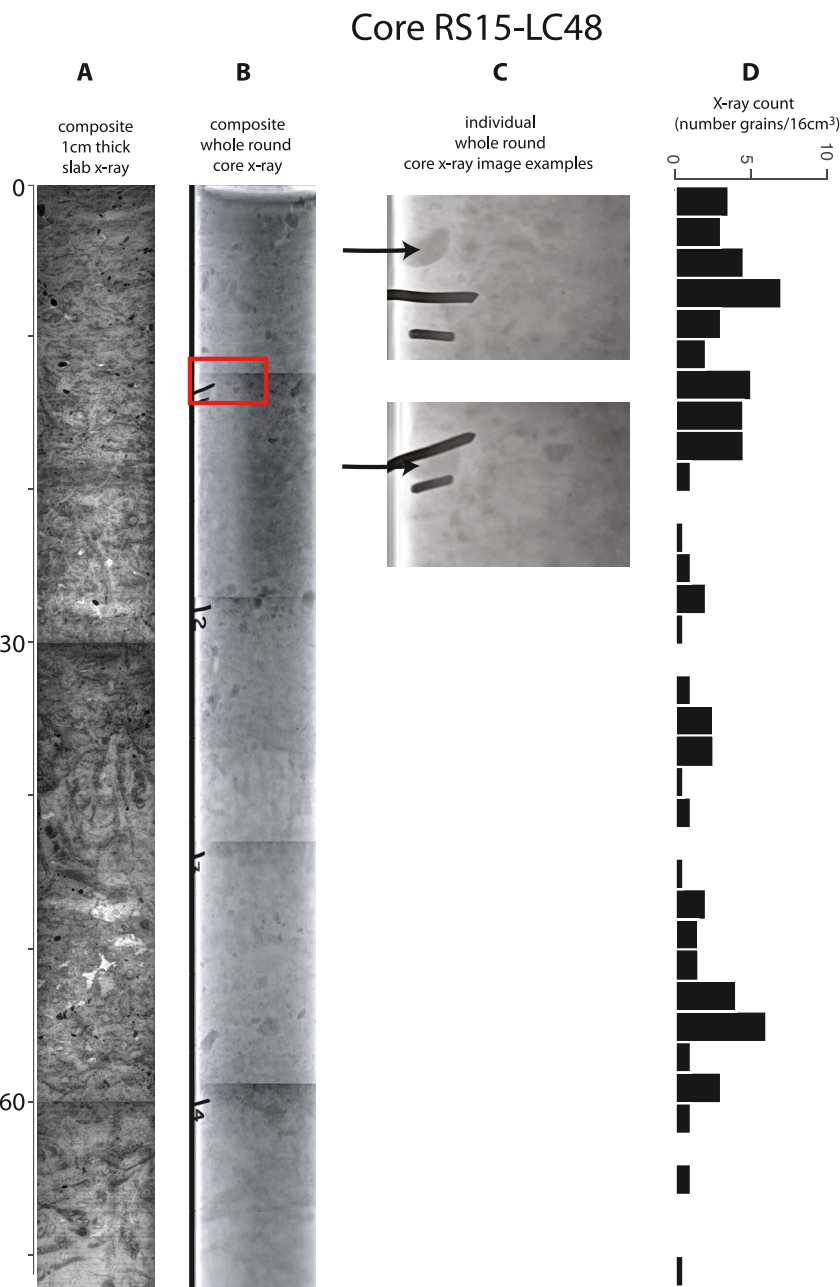


Figure 2. Representative example of X-radiograph images and counting results from RS15-LC48. (a) Composite image of separate 30 cm long x-radiograph of a 1-cm thick slab; (b) Composite X-radiograph from the whole round core. Reference markers (labeled 1–5) were placed every 15 cm on the core liner. These markers remained constant, while the core was moved relative to the x-ray source to obtain each image collected. (c) Zoom of separate images taken from whole round core (red box in b), with black arrows showing distortion of the image and apparent movement of a clast relative to the reference marker. (d) Counts of clasts >2 mm along the a-axis, as measured on the 1-cm x-radiograph “slab” images, binned into 2 cm intervals.

core face (cf. Weber et al., 2014), or opportunistic scanning of U-channel samples (cf., Cowan et al., 2008), as images obtained from a point source on half and whole round core often severely distort spatial measurements as the angle of the path x-rays take through the core will be highly variable, that is, a parallax effect (Croudace et al., 2006). This can result in difficulty in compiling a single composite image of a core derived from multiple x-ray measurements and can result in either the duplication, or deletion of objects near the edges of each image used to create the composite image (Figure 2). Finally, as this method commonly examines either a >1 or >2 mm fraction, the size being determined by that which can be reliably distinguished on x-radiograph images. Reliably

picking these grains is dependent on the quality of the image and contrast in density of the grains relative to the background lithology. In addition, similar to the sample availability issues for sieving and LPSA, some cores may also lack statistical significance in cores where IRD abundance of >2 mm grains is relatively low. Therefore, this approach is more suitable to regions of intense iceberg rafting (Grove, 1987; Weber et al., 2014).

Slab-based/U-channel sampling or line scan imaging largely overcomes the distortions inherent in imaging whole round cores with point-source x-rays. However, slab sampling is a (partially) destructive method, and where archive cores have already been sampled this is not an option. Nevertheless, these slabs/U-channels can subsequently be resampled for further analysis of the IRD or sediment (Cowan et al., 2008). Access to computed tomography (CT)-scan imaging is becoming increasingly accessible, and overcomes this obstacle (particularly on archive core halves) - but this is a computationally and financially expensive method, and not always logistically practical over hundreds of meters of drill core, or on legacy cores that have already been sampled. Finally, because this method commonly measures the gravel fraction (>2 mm), and some sediment cores, especially piston cores, have a narrow diameter (e.g., 66 mm for a standard Integrated Ocean Drilling Program cores (IODP) piston core), larger grains are not going to be sampled (e.g., cobbles) and will either be pushed out of the way by the advanced piston corer (potentially resulting in significant coring disturbance), or result in incomplete recovery.

3. Materials and Methods

3.1. Core Sampling and Description

To conduct the comparisons of the three IRD abundance methods, two sediment gravity cores (11 cm diameter) RS15-LC42 and RS15-LC48 were obtained by the Korea Polar Research Institute (KOPRI) Icebreaker R/V Araon in 2014/15 (Figure 1) from contourite drifts in 2,084 and 3,167 m water depth, respectively, in the Western Ross Sea. The cores were split, and visual core descriptions were undertaken aided by x-radiograph imaging (Jung et al., 2019; Ohneiser et al., 2019) and verified by quantitative grain size analysis using LPSA. For x-radiograph analysis, a 1-cm-thick, 8 × 30-cm slab was removed from the center of each split core section, placed within plastic plates and x-rayed. Discrete samples for sieve and LPSA were then collected from cores RS15-LC42 and RS15-LC48. RS15-LC48 was sampled approximately every 20 cm (total of 74 samples), and RS15-LC42 was sampled approximately every 10 cm (total of 121 samples). Each homogenized sample was subsampled for the sieve and LPSA analyses, and consequently each analysis for these methods is from identical depths. We intentionally selected cores for our IRD comparison study that are not ideal due to turbidite deposition and/or winnowing. However, because these processes are pervasive on the Antarctic continental margin records, we consider the chosen records to be the representative of a range of records used in IRD studies previously, and therefore relevant to defining the appropriate size-range cut-off and methods used to distinguish IRD. Consequently, the results presented in this study should not be used as records to define ice dynamics, unless further investigation of influences affecting concentration of the relevant size fraction is carried out.

For broader assessment of the significance of different Antarctic continental margin depositional settings, we assess the differences in results from CT-scan x-radiographs, LPSA and sieving methods at two sites where IRD records have been previously published using either sieve or LPSA to assess reproducibility between methods in these settings. These settings include a levee setting at Integrated Ocean Drilling Program (IODP) Site U1361 (water depth 3,465 m) offshore from Adélie Land, where overbank spill from canyon-focused cascading water flows and turbidity currents, is separated by prolonged periods of hemipelagic and pelagic sedimentation, suspended sediment deposition from contour currents, and ice-raftering processes (Escutia et al., 2011; Patterson et al., 2014). At this site, it has previously been noted downslope currents are too weak to extensively winnow the fine fraction, and while coarse sand grains and clasts (>2 mm) are absent in sand laminae (Patterson et al., 2014; Wilson et al., 2018). We also sampled a continental rise contourite drift obtained by Ocean Drilling Program (ODP) Site 1165 offshore from Prydz Bay (water depth 3,537 m; Figure 1), which is characterized by mudstones with thin silt laminae influenced by contour currents, interbedded with bioturbated diatom rich muds deposited via hemipelagic processes (O'Brien et al., 2001; Passchier, 2011.). All depths used in this study used the IODP CSF-B depth scale (in meters below seafloor; mbsf), which corrects for core recovery exceeding 100% due to expansion (Escutia et al., 2011).

3.2. IRD Counting From X-Radiographs

For the RS15-LC42 and RS15-LC48 cores, lithogenic grains >2 mm in diameter were identified visually in x-radiographs from 1-cm thick slabs with an 8 cm width. The stratigraphic depth and a-axis length of each grain was recorded using a custom-made script in Matlab™, and the number of grains >2 mm was then binned in 2 cm depth increments downcore, which results in a determination of number grains/16 cm³ (Figure 2). Correlation of the counts provided by the two users is $r = 0.961$ and $r = 0.927$ for cores RS15-LC42 and RS15-LC48, respectively.

For the ODP 1165 and IODP 1361 cores, grains >2 mm along their a-axis were measured from a 1 cm thick “composite slice” of stacked CT scan images obtained from the archive half of each core using HOROS open source software and binned into 2 cm intervals. ODP and IODP piston cores have a diameter of 6.6 cm, which results in a determination of number grains/13.2 cm³. However, in these cores, the two separate counts were conducted on composite slices that were offset by 5 mm (parallel to the core face) to assess reproducibility from slabs taken from different images within the CT-scan stack. Although the slabs are overlapping and ideally would have been offset by 1 cm, the round nature of the core meant a larger offset resulted in significant differences of the volume being measured. Correlation of the counts from these offset “slabs” provided by the two different users are $r = 0.696$ and $r = 0.814$ for cores IODP Site U1361 and ODP Site 1165, respectively. Where counts were different by more than four grains, these images were cross checked by each user, and in all cases verified to be real; for example, due to the presence of pebble nests/concentrations, or one large grain in one image containing multiple smaller grains in the other slab image.

These methodologies are broadly consistent with previous ship-based investigations of Antarctic continental margin sediments, with the abundance of material >2 mm considered an indicator of the content of IRD (Grobe, 1987). Two clast counts of the same x-radiographs for RS15-LC42 and RS15-LC48 were made by different operators to assess the influence of subjectivity (Figure 3). Subjectivity can arise from overlapping grains, or lower density grains occurring on a background of intense burrowing or lithological complexity (e.g., lenses of fine sand). An important point for obtaining reproducible results with this approach is that all operators are working with the same criterion for defining IRD. Without standardization of criteria it is inevitable that independent laboratory groups will generate different results depending on how they are trained to identify IRD. This “training” aspect will also influence automatic algorithm-based or machine-learning counting methods, which ideally have to be fine-tuned for any given site to account for different lithofacies, IRD grain density, overlapping grains, and core/x-radiograph quality. In this paper, the final IRD count data is an average of the two IRD count runs made by the two independent operators (Figure 3).

3.3. Sieve Analysis

Approximately 10–15 cm³ of dry sample (oven dried at 50°C for 24 hr) were initially weighed (~10–20 g) and then wet sieved at 250 µm. The >250 µm fraction was then dry sieved at 250 µm–2 mm and weighed. Each sample was then visually checked under a stereo microscope for biogenic components (biogenic silica, CaCO₃), and authigenic minerals. Removal of the biogenic component can potentially be determined by visual estimates through counting methods, but this adds a qualitative aspect to the IRD abundance calculation, when subtracting the biogenic percentages determined (Kanfoush et al., 2002; Murphy et al., 2002). This is because these estimates are volume-based, but the IRD abundance is weight-based, and as biogenic grains are composed of opal/carbonate and are highly porous/hollow, they are often orders of magnitudes less dense than lithogenic grains, so a volume-based estimate will not be proportional to weight-based estimates (Murphy et al., 2002). In order to maintain consistency in the weight-based estimates via sieving, we physically/chemically treated the >250 µm fraction.

To remove foraminifera, the samples were treated with ~20 mL of 10% hydrochloric acid (HCl) for approximately 2 hr to dissolve CaCO₃. Biogenic silica was removed from the coarse fraction by adding ~20 mL of 1M sodium hydroxide (NaOH) for a 72-hr period. The samples were heated in a water bath to 70°C and occasionally stirred (Lewis & McConchie, 1994). The washed samples were then dried, and final weights recorded. On reobservation, it was clear that large robust radiolaria tests survived the 1M NaOH treatment. These were subsequently removed by crushing the dry >250 µm fraction with very gentle finger pressure between two pieces of paper and then re-sieved. This method successfully crushed the fragile radiolaria with no destruction of the lithological fraction.

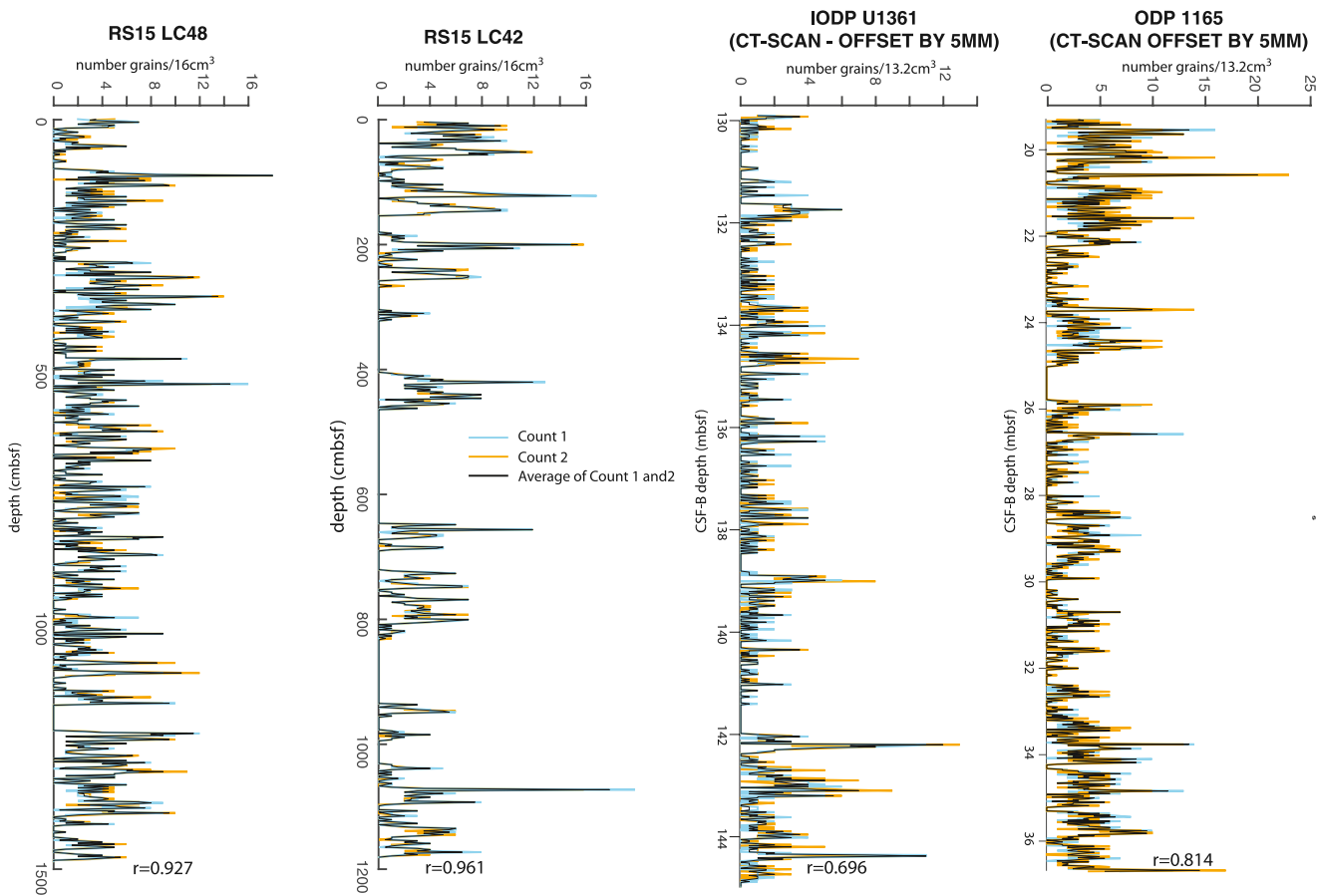


Figure 3. X-radiograph (x-ray) counts from cores RS15-LC48 and RS15-LC42, and CT-scan counts from ODP site 1165 and IODP site U1361. Count 1 (blue) and 2 (orange) were undertaken by two separate users, and the average value is shown (black). For cores RS15-LC48 and RS15-LC42, although there are minor differences in absolute values between users, the signals are consistent and correlation values are high. For cores ODP Site 1165 and IODP Site 1361, the correlation values and visual comparisons are likely lower because the images measured were different between users, that is, counts were from 1-cm thick composite slabs from CT-scans offset by 5 mm within the core face.

Consequently, this may provide a much more rapid and more appropriate alternative (or pretreatment) to chemical dissolution of biogenic silica in the $>250\text{ }\mu\text{m}$ fraction. However, it should be checked there are no fragile lithologies within the IRD fraction that could also be removed with this method. This is easily assessed through visual examination of the $<250\text{ }\mu\text{m}$ fraction after sieving.

3.3.1. Reproducibility of Sieve Analyses

We also conducted reproducibility experiments on 25 samples from ODP Site 1165, with a volume of 10 cm^3 for each replicate sample (Figure 5g). The results show very high reproducibility with an R -value of 0.95. Although the residual plot (the difference between two independent analyses of the same samples) shows that there is greater variance at weight percentages above 6% (values range between 6% and 10%), no other systematic biases exist in this distribution indicating good reproducibility is obtained by this method at this site. The greater variance at weight percentages above 6% suggest some statistical significance issues result from the presence of higher numbers of very coarse sands ($>1\text{ mm}$) in a relatively small sample size.

3.4. Laser Particle Size Analysis

3.4.1. Pretreatment and Analytical Procedure

Although some LPSA measurements are analytically limited to measuring 0.15–0.9 g of sediment in the mud-rich sediments of this study, prior to analysis we pre-treated 2 g of bulk sample to avoid biasing samples to minor

lithological components (e.g., sand lenses or laminae). Processing of this amount of sample also readily allows for reproducibility experiments to be conducted. Biogenic carbonate was removed with 10% HCl for approximately two hours, and organic matter was subsequently removed by adding ~20 mL of 27% hydrogen peroxide (H_2O_2) to the bulk samples for a 72-hr period, heating them in a water bath at 70°C (Lewis & McConchie, 1994), and then washed/centrifuged three times in 18MΩ water to remove the remaining H_2O_2 and reaction product. Visual examination of smear slides of the RS15-LC42 and RS15LC-48 samples reveals <20% biogenic silica content. Biogenic silica was removed by adding ~20 mL of 1M sodium hydroxide (NaOH) for a 72-hr period in a 70°C water bath and occasionally stirring the samples (Lewis & McConchie, 1994). Smear slides were assessed to determine if biogenic silica dissolution was complete. The samples were washed in 18MΩ water and centrifuged at 4,700 ppm three times, and the supernatant was decanted and replaced with fresh 18 MΩ water following each of the treatments.

Prior to analysis the samples were subsampled (~0.15–0.9 g dependent on the mud content) to obtain an optimal laser obscuration (6%–14%) for the Beckman Coulter LS 13 320, with an aqueous liquid module (which circulates the sediment within a water volume of 1.25 L). The cone-and- quartering-method of dry, processed sediment was used for the subsampling (Lewis & McConchie, 1994). This technique involves mixing and evenly dividing the sample into smaller quantities, which ensures representative subsampling for the entire range of grain sizes. The subsamples were then dispersed in ~50 mL of 0.5 g/L sodium hexametaphosphate and agitated in a beaker placed in an ultrasonic bath for a minimum of 20 min. The samples were then immediately analyzed on the LPSA for 60 s, with no use of an ultrasonic probe, which could potentially damage sand grains.

The laser was re-aligned, and the background was measured before every sample, and the detector offset was measured every 30 min. The resulting measurements were converted to grain size using the QuartzNatural.rf780d optical model, which assumes all material has a refractive index of quartz suspended in water. Glass bead informal standards (250, 68, and 24 µm modal sizes) were run at the beginning and end of every day to check the instrument was operating correctly.

3.4.2. Assessment of Biogenic Silica Removal

Biogenic silica measurements confirm smear slide observations that the biogenic silica content ranges between 10% and 17% by volume in these samples. Numerous samples in the sieve analysis indicated robust radiolarians >250 µm in size survived NaOH digestion and required physical removal by gentle crushing. However, weight-based estimates of coarse fractions are less likely to be biased by low abundances of sand-sized diatoms and radiolarians, as they have a very low density and weight compared to terrigenous grains. This is because diatom frustules and radiolaria tests are hollow compared to a grain of quartz and are composed of highly porous biosiliceous material. These can be readily examined and removed in sieve-based methods. Due to these large density differences, moderate amounts of radiolarians/diatoms will have minimal influences on the weight of the coarse fraction, but despite this we still recommend that sieve-based methods physically/chemically remove biogenic particles, rather than estimating the weight difference via volumetric based assessment from microscope counting. However, as the underlying measurements in LPSA are volume-based, even small amounts of biogenic silica could significantly impact measurements. Thus, successful removal from all size fractions should be carefully assessed when undertaking LPSA measurements.

Three samples from RS15-LC48 were analyzed in triplicate to assess the extent of opal dissolution with different concentrations of NaOH. The first set of subsamples was an untreated control sample; the second set of subsamples was treated with ~20 mL of 0.2 M NaOH solution (cf. Passchier, 2011); the third set with 1M NaOH (cf. Patterson et al., 2014). This concentration is a more aggressive treatment and was expected to more efficiently remove biogenic silica, but may also have the potential to damage some clay minerals (Carroll & Starkey, 1971; Müller & Schneider, 1993) which we discuss below.

Smear slides of each sample were examined under a microscope after treatment. All samples treated with 0.2 M NaOH contained common siliceous sponge spicule fragments and partially dissolved diatoms (Figure 4). Smear slides of the 1M NaOH treatment showed almost complete dissolution of biogenic silica with rare instances of wispy “spines” and diatom fragments. Scanning Electron Microscope (SEM) images also show only rare

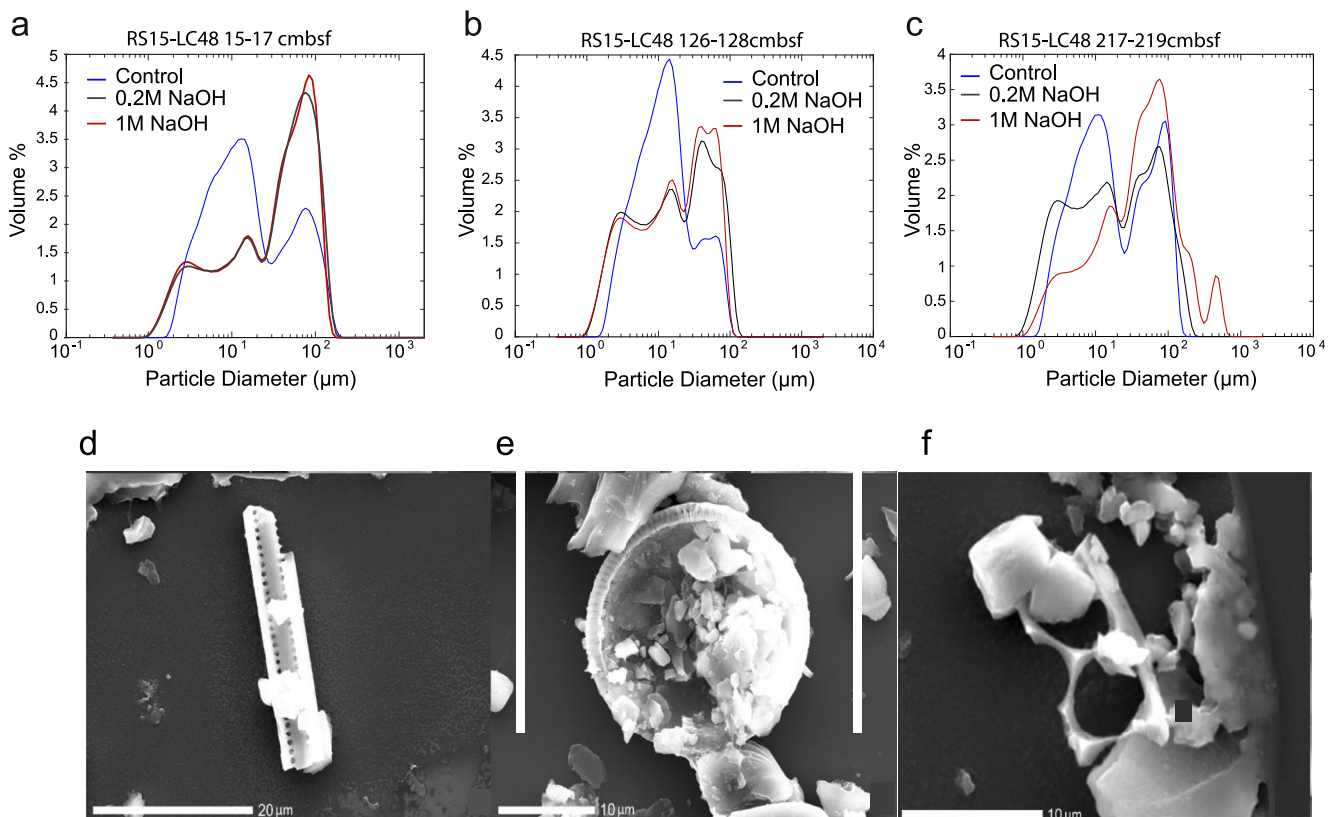


Figure 4. (a)–(c) Grain size frequency curves for three representative samples from core RS15-LC48 that were subsampled three times. Each subsample was treated with 0.2 M NaOH and 1M NaOH solutions, and a control with no NaOH treatment. (d) and (e) SEM images of diatom content in RS15-LC48 after 0.2 M NaOH treatment. (f) SEM images of diatom content in RS15-LC48 after 1M NaOH treatment.

fragments of diatoms observed in the 1M NaOH treated samples, but with whole diatoms still present in the 0.2 M NaOH treated samples (Figure 4).

The concentration of NaOH used to digest biogenic silica has a large effect on the grain size frequency curves (Figure 4). Two of the samples treated with 0.2 M NaOH solution have a similar grain-size frequency distributions to that of 1M NaOH treatment, suggesting complete dissolution where the biogenic silica content in the bulk samples is relatively low (Figure 4). However, the results of sample 217–219 cmbsf indicate that more aggressive treatment was needed to completely remove biogenic silica from this sample (Figure 4). We also emphasize that the percentage of biogenic silica in the bulk sample alone may not be a reliable estimate for the strength of treatment required as some genera of diatoms and radiolaria are more susceptible to dissolution than others (Ryves et al., 2001). In our samples, the majority of biogenic silica dissolved with 0.2 and 1M NaOH treatment occurred in the fine-grained (<63 µm) fraction, which is consistent with the grain size distribution of biogenic silica particles in Antarctic margin sediments (Pudsey, 2002; Warner & Domack, 2002). The similarity of the 0.2 and 1.0 M results in the two samples with low observed biogenic silica (Figure 4) also indicate that for our samples the increased strength of 1M relative to 0.2 M NaOH treatment is not causing additional damage to clay minerals in these samples. However, there remains the possibility that clay minerals susceptible to NaOH leaching may completely have been dissolved at 0.2 M NaOH leaching, and thus this could add additional error when comparing %IRD relative to the total sediment population using the LPSA method relative to other methods.

We note there is a fining of grain size in the clay fraction between the NaOH-treated and untreated samples for all samples we treated. While this could result from breakdown of clay minerals or biogenic opal to a finer grain size, we view this as unlikely because the distributions are consistent between 0.2 and 1 M NaOH treatments. If biogenic opal or susceptible clay minerals were still present after 0.2 M NaOH treatment, additional breakdown/dissolution would be expected in all samples with the stronger 1M treatment, but only the sample RS15-LC48,

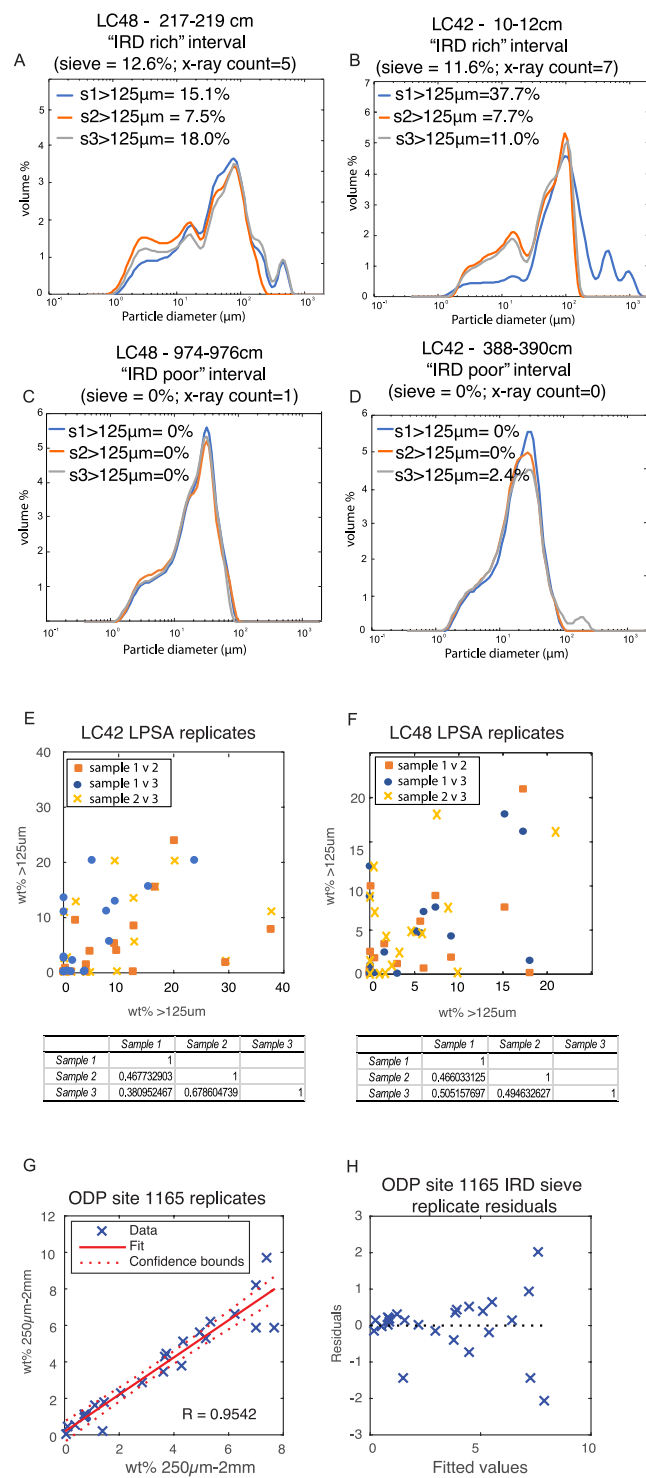


Figure 5. (a)-(d) Representative examples of repeat measurements on separate subsamples (replicate samples) using the Laser Particle sizer in cores RS15-LC42 and RS15-LC48. Note the lower reproducibility in the coarse fraction ($>125 \mu\text{m}$) in samples described as "IRD-rich," as identified in other counting methods. Good reproducibility is shown in the fine fraction ($<125 \mu\text{m}$) for both IRD-rich and IRD-poor samples. (e) Cross plot of replicate sample runs for RS15-LC42 > 125 μm LPSA measurements, with Pearson pairwise linear correlation coefficients (R values) matrix below. (f) Cross plot of replicate sample runs for RS15-LC48 > 125 μm LPSA measurements, with Pearson pairwise linear correlation coefficients (R values) below. (g) Cross plot of results of replicate sieving analyses ($>250 \mu\text{m}$) of samples from ODP Site 1165, with linear regression model and 95% confidence bounds. Each replicate comprised $\sim 10 \text{ cm}^3$ volume. (h) Plot of residuals versus fitted values from the linear regression model for the replicate sample runs from ODP Site 1165.

217–219 cm showed this (Figure 4). Consequently, we propose the more likely cause of this fining is that smoothing procedures in LPSA software are designed to model log-normal distributions around specific modes (Blott & Pye, 2006). The dissolution of biogenic opal in the silt fraction results in a lower mode at that size range, and a broader-shaped distribution would be expected if that mode was muted after dissolution (see Section 3.4.3 for more details on these software considerations).

A final caveat here is that sand-sized biogenic silica may be more resilient to dissolution and is less likely to be observed on smear slides – a result that we also observed in the sieving procedure where radiolaria survived a 1M NaOH treatment. Therefore, periodic sieving of treated subsamples should be conducted in biogenic-rich sediments to assess if biogenic silica is present in samples otherwise to be analyzed by LPSA. Such radiolaria may account for the single outlier peak in the coarse sand fraction for the 1M NaOH experiment in RS15-LC48 217–219 cm. However, in this particular sample such peaks are not seen in the untreated or the 0.2 M treated samples, and therefore this could represent a single-sand grain of 450 µm diameter in that one sub-sample.

3.4.3. Reproducibility Test of Laser Particle Size Analyzer in IRD-Bearing Sediment

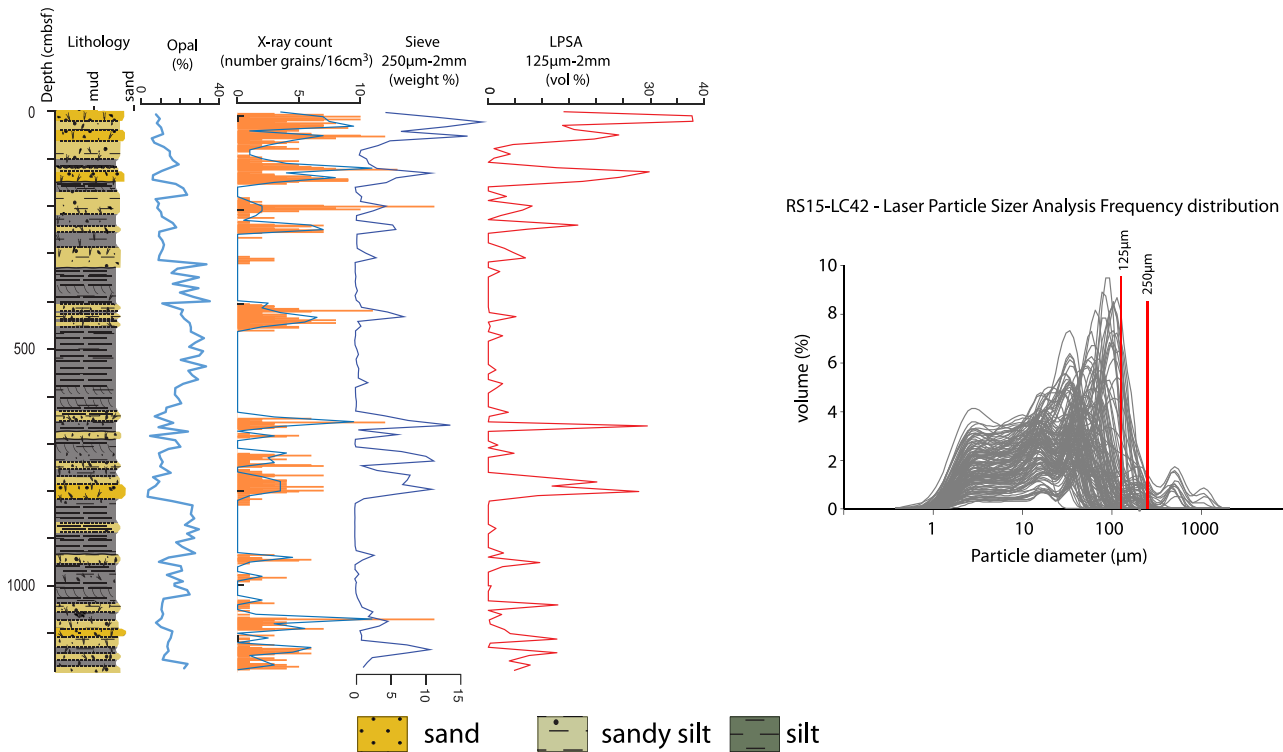
To determine the reproducibility of the LPSA to characterize medium to coarse sand fraction in mud-rich samples, 18 repeat samples for RS15-42 and 16 repeat samples for RS15-48 were run, where each sample was subsampled into three aliquots (from dry samples) and analyzed in the LPSA after biogenic and organic treatment had been completed. Samples with material >125 µm (e.g., potential IRD) in size (Figures 5a and 5b) showed lower reproducibility. Samples with no >125 µm grains all showed good reproducibility (Figures 5c and 5d), suggesting poor sample homogeneity across subsamples is the main cause of poor reproducibility. Reproducibility of the <63 µm fraction was good in all samples (Figure 5), indicating that the low number of out-sized sand grains in mud-rich sediment on the LPSA is the cause of the poor reproducibility in the >125 µm fraction. Sample 10–12 cm in RS15-LC42 displayed high IRD values in sieve and x-radiograph analyses, but highly variable IRD values in the LPSA 125 µm–2 mm method. While Samples 1 and 2 have high 125 µm–2 mm values (7.7% and 11%, respectively), most of this size range in the LPSA data is on the shoulder of a well sorted sand mode at 110 µm, with no values >250 µm. However, Sample 3 in the replicate tests, shows two modes in the IRD fraction, at ~500 and 1000 µm, which likely represent outlier IRD grains. These outliers appear to have significantly affected the entire distribution of the <250 µm fraction (e.g., note widening of the distribution around the 110 µm mode). This is likely a function of the problems associated with the LPSA software models assuming a log-normal distribution (Blott & Pye, 2006), when the real sediment populations in glacial settings do not contain such a distribution, with potentially single occurrences of outlier grains in the coarse sand fraction being overestimated.

3.5. Statistical Tests

We use bivariate cross plots with linear fit regression models to assess relationships between the different methods and reproducibility. For LPSA and sieve data, each discrete sample was from identical depths (see Section 3.1), while for the x-radiograph data we re-binned the raw count data so that that bin edges matched the top and bottom depths of the discrete LPSA/sieve samples (Figure 6). Pearson pairwise linear correlation coefficients (*R*-values) are used to quantify goodness of fit. However, *R*-values should not be used in isolation, as *R*-values can be strongly influenced by outliers. This influence is evident in plots of residual values against the linear fit model, which is a measure of the distance of a given data point from its predicted value based on the linear fit model. More confidence can be placed on correlation when high *R*-values coincide with a residual plot that forms a relatively random distribution of points above and below the 0-line value of residuals, with minimal outliers.

Linear regression lines are also calculated, and regression lines where the intercept passes closer to the origin are interpreted to demonstrate a better consistency between methods. This is because each method has different size ranges, and therefore assessment of the distance that regression lines intercept from the origin provides a measure of whether one method (and size cut-off) is less sensitive to the measuring of potential IRD than the other method; for example, the LPSA versus x-radiograph cross plots for RS15-LC42 and RS15-LC48 indicate the LPSA measurements more regularly show a complete absence of 125 µm–2 mm grains, where x-radiographs indicate >2 mm grains are present. Such a relationship results in the regression line intercepting above zero on the x-radiograph count axis and that the x-radiograph count is more sensitive at measuring IRD in these cores

Core RS15-LC42



Core RS15-LC48

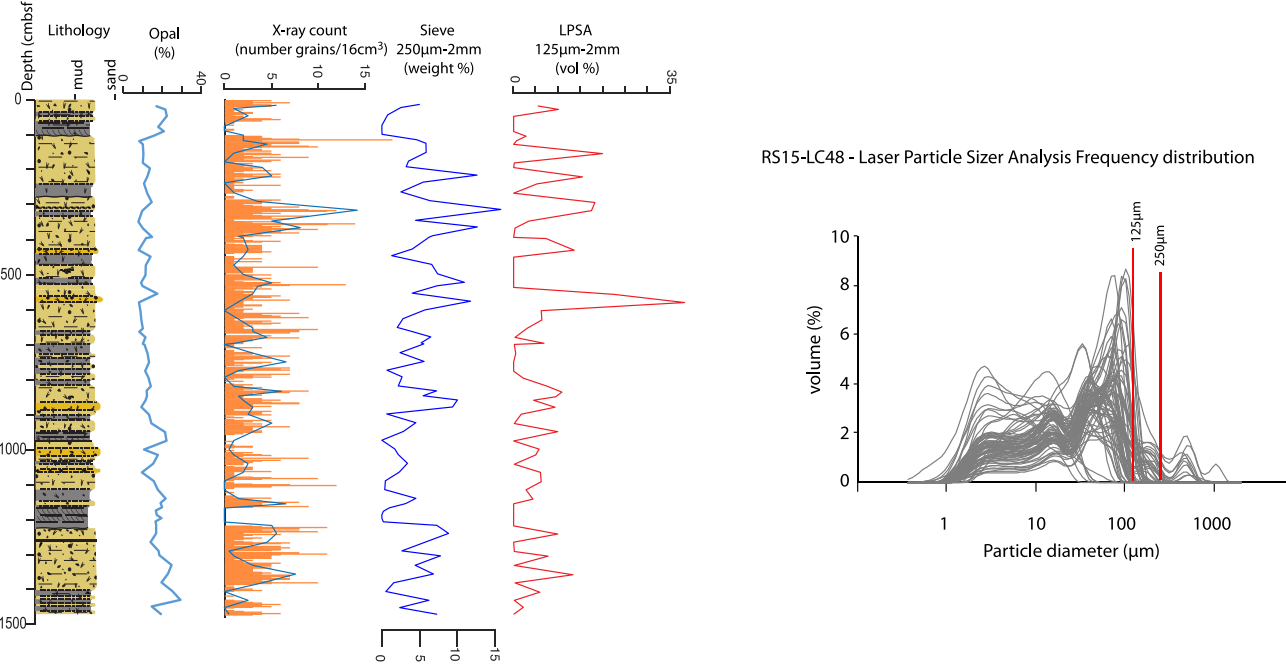


Figure 6. Lithological columns (after Ohneiser et al., 2019), biogenic opal %, coarse fraction grain size analysis, and LPSA grain size measurements from cores RS15-LC42 (top row) and RS15-LC48 (bottom row). Grain size analysis shows number of clasts (>2 mm) counted on x-radiographs (x-ray count), percentages of the terrigenous fraction 250 μm–2 mm obtained by sieving, and volume percentages of the biogenic-free fraction 125 μm–2 mm as determined by LPSA. The x-radiograph (x-ray) counts are shown as binned values as number of grains over a 2 cm core depth interval (orange bars), and values interpolated to the same depths as the sieve and LPSA values (gray lines).

(Figure 7). This is also identifiable in the residual plot by a wide scatter of residual values at the intercept value on the fitted values axis. Such relationships provide insights into whether further investigation of the grain size distributions is required to determine if an over-estimate is picking up non-IRD (e.g., turbidite sands), or if the under-estimate is not sensitive enough to record IRD in a statistically significant manner (e.g., a small sample volume).

4. Comparison of the IRD Methods

The three published analytical methods compared in this study to determine the “coarse-grained” content for cores RS15-LC42 and RS15-LC48 all utilize different grain size limits to determine the IRD component. In this section, the apparent differences in IRD content attributable to using different size limits between these methods are quantified by comparing downcore variation between 125 µm and 2 mm (volume % using LPSA), 250 µm–2 mm (weight % by sieving) and >2 mm (clast counts in x-radiograph images) estimates.

4.1. RS15-LC42 Comparison of X-Radiograph, Sieve, and LPSA Methods

A qualitative visual assessment of RS15-LC42 shows a good comparison between all three methods in most sections of the core, but some sections show large discrepancies (Figure 6). For example, between 400 and 453 cmbsf and 720 and 760 cmbsf, the LPSA method is less consistent in registering higher values in the 125 µm–2 mm fraction than the more persistent elevated values evident in the sieve (250 µm–2 mm) and x-radiograph data (>2 mm; Figure 6). A linear regression model was applied to the cross plot of the various methods (Figure 7). The strongest correlation coefficient value occurs in the sieve and LPSA regression (R -value = 0.758). However, the cross plot and residual plot also demonstrate there are some biases in this correlation, with a large number of LPSA >125 µm measurements yielding 0% when the sieve method contains up to 11% by weight in this size class (Figure 7), but low sieve values more generally correspond to low LPSA values. This indicates the LPSA more commonly underestimates the IRD fraction (as defined by the >125 µm fraction) at this site when compared to the sieve data IRD fraction (as defined by the >250 µm fraction). A near identical bias is observed in the comparison of LPSA versus x-radiograph counts (Figure 7), but some relatively high LPSA values also correspond to 0 values in x-radiograph counts. However, in general the LPSA versus x-radiograph method comparison also demonstrates a good correlation, but is lower (R -value = 0.527) than the LPSA versus sieve. The correlation of sieve versus x-radiograph data has an R -value of 0.677, while the residual plots demonstrate less bias in distributions, but the x-radiograph method may slightly underestimate IRD content because 0 values can correspond to sieve weights up to ~3%. Despite these biases, these results indicate the LPSA, sieve and x-radiograph methods are relatively consistent in identifying IRD grains at this site.

For some samples, the LPSA data indicate IRD presence, whereas the sieving analysis does not. However, grain size frequency distribution curves demonstrate the samples are mostly sandy silt, with some samples showing a well-sorted sand mode between ~63 and 100 µm. The coarse shoulder of this mode passes into the 125 µm fraction in numerous samples, but at sizes above 250 µm there is an irregular distribution of coarser particles (Figure 6).

4.2. RS15-LC48 Comparison of X-Radiograph, Sieve, and LPSA Methods

The qualitative visual assessment of RS15-LC48 size data also shows a reasonable comparison between all three methods but with intervals where there are large discrepancies. The LPSA method shows two anomalously high data points between 550 and 580 cmbsf, as well as an under-sensitivity to recording grains between 125 µm and 2 mm (e.g., 499–535 cmbsf), compared to the other two methods and their respective size fractions (Figure 6). The R -value of 0.175 demonstrates minimal correlation between the x-radiograph and LPSA methods and is also lower for the LPSA versus sieve comparison (R = 0.417) than for site RS15-LC42 (Figure 7). Residual plots for both of the cross plot comparisons to LPSA measurements show distinctly biased distributions caused by the LPSA 125 µm - 2 mm measurements consistently showing 0% values when the sieve and x-radiograph methods for estimating IRD (250 µm and 2 mm) indicate higher values (Figure 7).

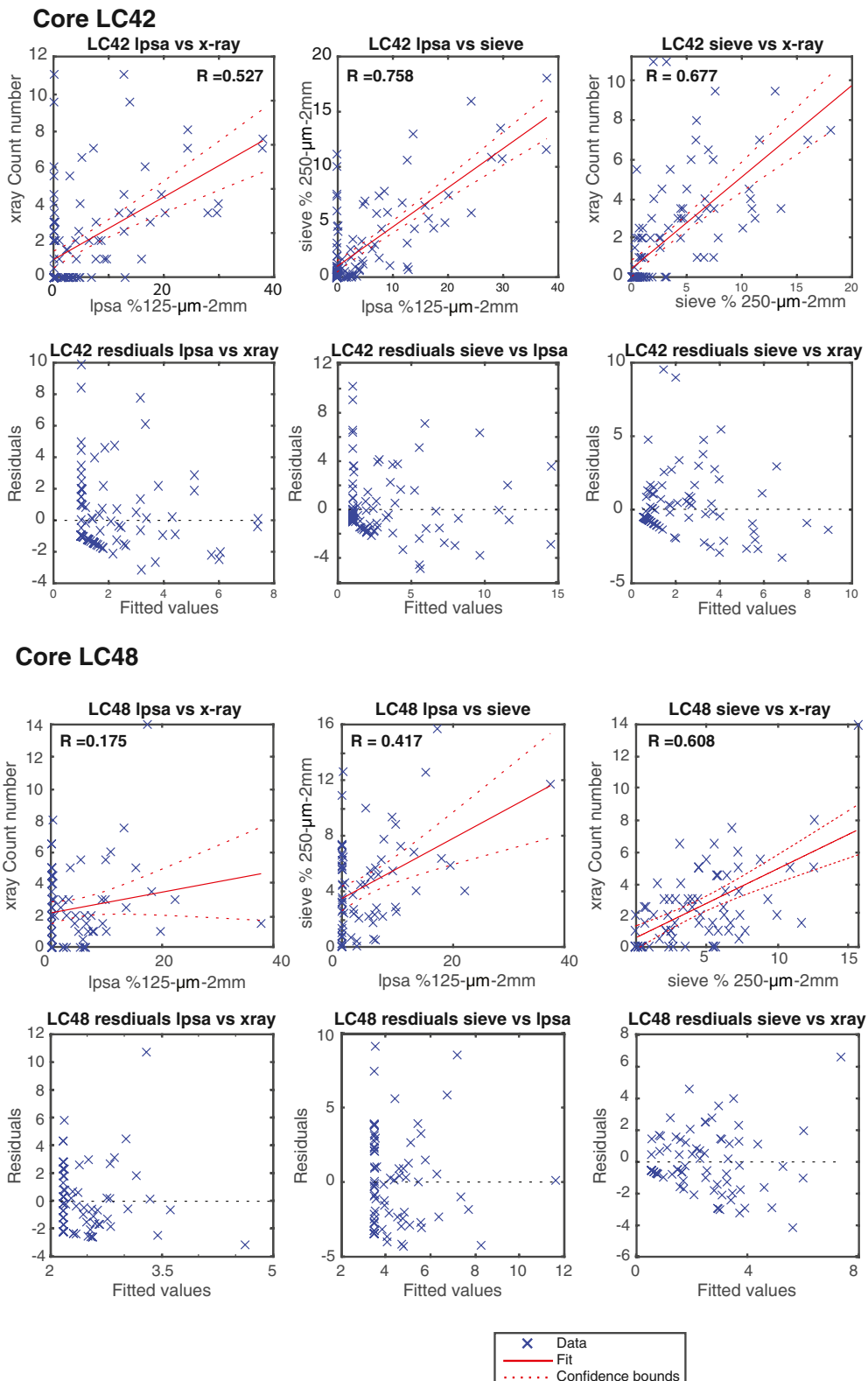


Figure 7. (Top row) Cross plots of x-radiograph (x-ray count) clast values, sieve-based weights of 250 μm –2 mm, and 125 μm –2 mm LPSA analysis for RS15-LC42, with linear regression model and 95% confidence bounds. (Second row) Plot of residuals vs. fitted values from the linear regression model for cross plots shown in top row. (Third row) Cross plots of x-radiograph (x-ray) count values, sieve-based weights of 250 μm –2 mm, and 125 μm –2 mm LPSA analysis for RS15-LC48, with linear regression model and 95% confidence bounds. (Bottom row) Plot of residuals vs. fitted values from the linear regression model for cross plots shown in third row.

Both cross comparisons with the LPSA indicate that the regression line intercept is offset from the origin, further suggesting the LPSA is less sensitive to measuring potential IRD at this site, when compared to the sieve and x-radiograph methods. The sieve versus x-radiograph correlation at RS15-LC48 has the highest *R*-value of 0.608 with a gradient that passes close to the origin. The residual plots demonstrate less clear biases in the distributions, with an even distribution of residuals across a range of fitted values. This indicates the sieve and x-radiograph methods demonstrate a more reliable consistency in identifying potential IRD grains (as defined by various differences in size fractions) at site RS15-LC48 than the LPSA.

As for RS-LC42, the LPSA data indicate IRD presence in some samples, whereas the sieving data indicate absence of IRD. Grain size frequency distribution curves for RS15-LC48 demonstrate the samples are mostly sandy silt, with some samples showing a well-sorted sand mode between ~63 and 100 μm . The shoulder of this mode passes into the 125 μm fraction, but this influence is greatly reduced when compared to RS15-LC42 distributions. At sizes above ~250 μm , there is an irregular distribution of coarse grained particles that is more consistent with a coarse tail distribution of IRD (Figure 6).

4.3. IODP Site U1361 Comparison of X-Radiograph, Sieve, and LPSA Methods

We analyzed sieve and LPSA data, as well as x-radiograph images from CT scans in the 130 to 146 mbsf interval of U1361 (Figure 8), which is stratigraphically below that studied by Patterson et al. (2014), but the range of facies and depositional processes appear similar (Escutia et al., 2011). Facies assemblages at IODP Site U1361 consist of finely laminated muds, massive and bioturbated muds, and are interpreted as representing deposition by non-erosive spill-over of low density turbidity currents or cascading water masses, as well as hemipelagic and bottom current influenced deposition (Escutia et al., 2011). The non-erosive, and gradual depositional nature of these spill-over deposits, alongside a relatively consistent sedimentation rate has allowed previous studies to use the IRD records at this site to infer past shifts in ice sheet dynamics (Patterson et al., 2014). Our datasets indicate a poor visual comparison between the sieve (250 μm –2 mm) and the LPSA (125 μm –2 mm) values (Figure 8). One sample was extremely high in all measurements (at 142.46 mbsf), and when included in the correlation analyses produced a high correlation value. However, when this one point is excluded (alongside a short 55 cm long interval that was u-channelled; Figure 8), the sieve versus LPSA correlations have an *R*-value of 0.3343, with a large number of LPSA measurements having 0 values when the sieving shows up to ~1.3%wt, and vice versa some high LPSA value coincide with low sieve values (Figure 8c). The grain size frequency distribution curves indicate samples contain well sorted sands with modes displaying shoulders that cross into the 125–250 μm fraction. This is inconsistent with the “coarse tail” distribution shown in the frequency curves from RS15-LC42 and RS15-LC48 (Figures 6 and 8b), and is more consistent with sand laminae deposition from an overbank levee turbidite (Strachan et al., 2016). The grain size frequency distribution also indicates most of the U1361 samples have a small, but persistent well sorted sand mode between 125 and 250 μm , with very few samples containing grains exceeding 250 μm in size. Such a mode is potentially more consistent with turbidite or other non-IRD origin. The LPSA data indicates that the shoulder of the well-sorted sand mode does extend marginally into >250 μm fraction, which could add a small amount of noise to the IRD estimates when using 250 μm as the lower limit cut-off in sieving. However, previous works have shown that the LPSA modeling assumption of a log-normal distribution is not always valid at these size ranges, and sieve data can show a more skewed distribution that do not extend as broadly into these coarser grain sizes (Blott & Pye, 2006). Consequently, while these LPSA software modeling artifacts will by default affect the LPSA estimates, they may not affect the sieve-based estimates. For samples where the influence of these shoulders is ambiguous in sieve data, visual or quantitative estimates of sorting in the coarse fraction could be used to assess if a non-IRD grain size populations is influencing the >250 μm fraction.

The CT-scan x-radiograph counts also showed the lowest reproducibly in the cores used in our study (Figure 3). As these counts were from profile “slices” taken at different (but overlapping) depths in the core face, and count numbers per 2 cm bin were often less than 2 grains, this suggests there may be a statistical significance issue with the small volume of sediment being measured in these 1 cm slabs, in combination with the relatively low concentration of IRD in this core example. With CT-scans, this issue could be potentially overcome by measuring a thicker composite slab through the entire core volume, which may result in overlapping grains being counted (particularly in automated methods), but in cores with low abundances, these could be visually assessed via

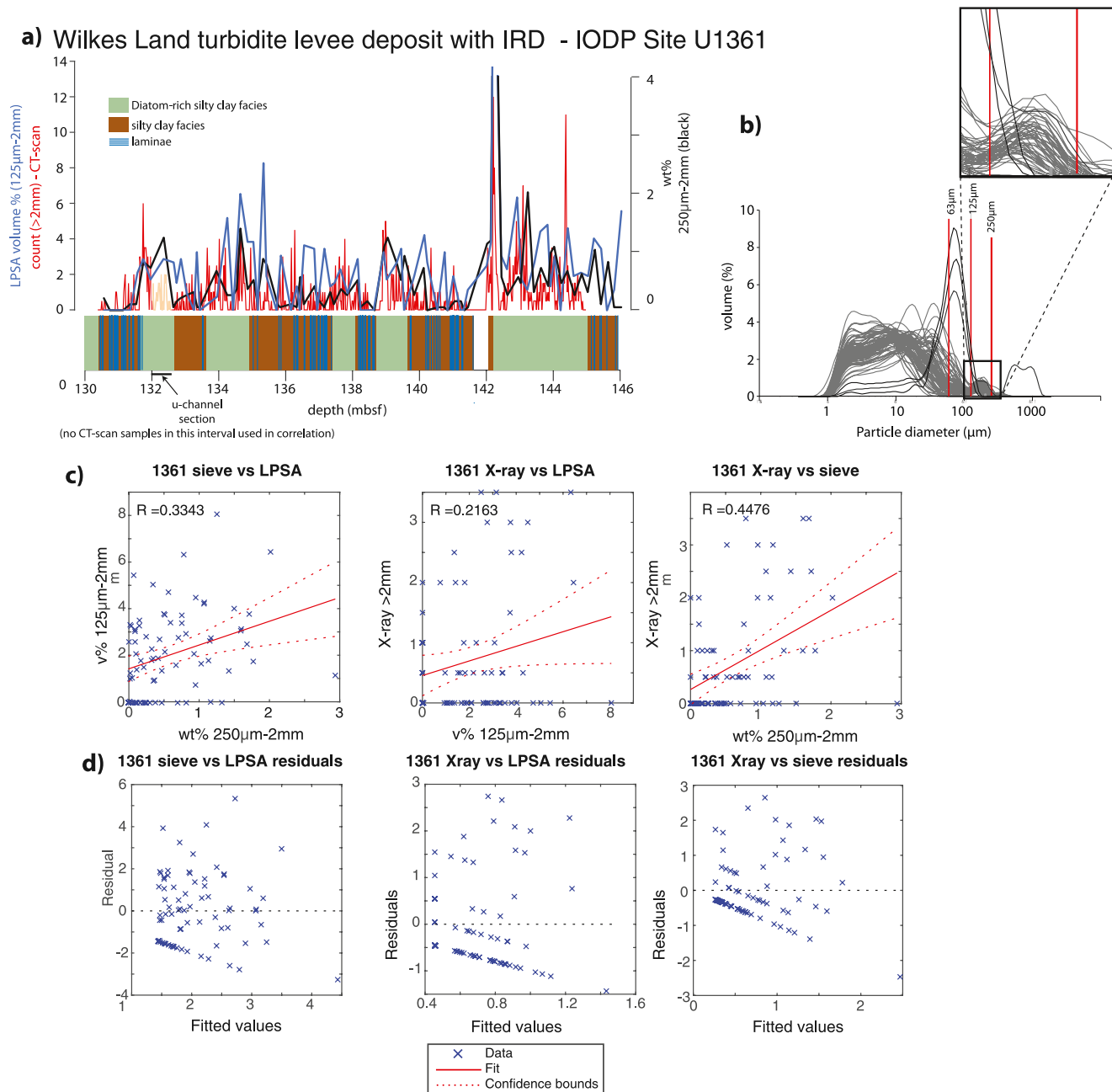


Figure 8. (a) Downcore comparison of coarse fraction content measurements from sieve ($>250\text{ }\mu\text{m}$), LPSA methods (>63 and $125\text{ }\mu\text{m}$) and x-radiograph (x-ray) methods at IODP Site 1361, an levee setting on the lower continental rise offshore from Adélie Land (Escutia et al., 2011); Lithological column follows lithofacies classification scheme of Patterson et al. (2014), with laminae mapped to depth from core photos, and adjusted to the CSF-B depth scale to correct for core expansion. (b) Grain size frequency distributions of the LPSA measurements shown in panel (a); (c) Cross plot of sieved-based measurements of $>250\text{ }\mu\text{m}$ weight percentages and LPSA $>125\text{ }\mu\text{m}$ percentages, with linear regression model and 95% confidence bounds. (d) Plot of residuals vs. fitted values from the linear regression model for plot in panel (c).

secondary analysis of the 3D CT-scan images. The x-radiograph versus sieve method correlations are the strongest in the set of comparison ($r = 0.4476$), which is also apparent in visual examination of the datasets (Figure 8a). This statistical significance issue is evident in many x-radiograph count values being 0 when sieve estimates are sensitive to recording grains, alongside the different CT-scan composite slabs showing lower correlation ($r = 0.696$; Figure 3). The LPSA versus x-radiograph method correlation is the weakest ($r = 0.2163$).

4.4. ODP Site 1165 Comparison of X-Radiograph, Sieve, and LPSA Methods

Similar to U1361, we investigated sieve and LPSA data alongside CT-scan x-radiograph images at this site. We analyzed the 20 to 36 mbsf interval of ODP Site 1165 by sieving grains over 250 μm in diameter, for samples as close to the same depths for the LPSA measurements presented by Passchier (2011) as remaining sample availability would allow. Despite a slight offset in some samples, our datasets still indicate a very good visual correlation between our x-radiograph (>2 mm) and sieve (250 μm –2 mm) data, and the LPSA (125 μm –2 mm) results presented by Passchier (2011) (Figure 9). This is demonstrated by an *R*-value of 0.7 for sieve versus LPSA measurement. Compared to the other sites studied by us, the LPSA 125 μm –2 mm shows better consistency with the other methods in measuring coarse grained particles. Although there are still numerous samples that show 0% when sieving >250 μm gave values up to 2%, this bias is more subdued in the residual plot when compared to the other sites investigated in this study (Figure 9).

The CT-scan x-radiograph counts were binned to the same depths as LPSA and sieve samples, respectively, and also showed the higher reproducibly in this core compared to U1361. We interpret the higher correlation here in the CT-scan data to be the consequence of the higher gravel content resulting in this size fraction having higher statistically significance, which is also displayed by the higher correlation between the two counts for the CT-scan images (Figure 3). The x-radiograph versus sieve methods have a good correlation ($r = 0.515$), which is also apparent in visual examination of the datasets (Figure 9). The LPSA versus x-radiograph methods show the weakest correlation ($r = 0.385$). Despite these correlation values, the qualitative visual comparison appears strong between all three datasets, albeit with an increased sensitivity to measuring the coarse fraction between 125 μm and 2 mm when compared to the x-radiograph counts of grains >2 mm. This increased sensitivity is evidenced by the slope of the linear regression in the cross plot (Figure 9b). The residual and cross plots show less systematic biases when compared to the other sites in this study.

5. Discussion

5.1. Implications of Methodology on Estimating IRD Percentages

The results of this study indicate higher correlations between IRD percentage determined by sieve analysis (250 μm –2 mm) and visual clast counts using x-radiograph analysis (>2 mm). Although good correlations can also be clearly identified with the LPSA data and the other two methods in many cases, it generally displays a weaker relationship to the x-radiograph method (Figures 7–9). The grain size frequency distribution curves (Figures 6 and 8) show that the >125 μm fraction is potentially capturing the coarse-grained shoulder of well-defined modes in sandy silts and silty sands in the samples we analyzed. As discussed earlier, this well-defined mode is more consistent with turbidite silt/sand beds noted in the visual descriptions of the U1361 core (Escutia et al., 2011). Although this fraction is undoubtedly capturing an IRD component, it is apparent that at such levee sites on the Adélie Land margin and contourite drifts in the Ross Sea, the >125 μm LPSA method may be overestimating the IRD component of sediments by incorporating part of a size mode likely deposited or concentrated by other processes. Consequently, although it may capture a significant IRD signal, it is also likely to result in a noisier signal.

Examining these distributions, the >250 μm fraction as measured by the LPSA instead could potentially reduce the spurious peaks associated with the shoulder of the sandy silts and silty sand modes. However, another key feature of the LPSA comparisons to the other two methods is that it also fails to regularly detect any sediment in this size fraction, whereas both sieve and X-radiograph analysis consistently show measurable amounts (Figures 6, 8 and 9). Our tests on LPSA measurements demonstrates high reproducibility in the mud to fine-sand fraction, but lower reproducibility for the >125 μm fraction due to the sample sizes being measured, and consequently raising the grain size threshold to 250 μm is not likely to resolve this issue.

The larger sample size of 10–15 cm³ of dry sample (10–20 g) used for dry sieving appears to show that the 250 μm –2 mm grain size fraction at site 1165 (Figures 5g and 5h) has good statistical significance ($r = 0.95$), alongside better correlation to the x-radiograph data ($r = 0.45, 0.51, 0.61$, and 0.68) for cores IODP U1361, ODP site 1165, RS15-LC48, and RS15-LC42, respectively. The issue of subjectivity in x-radiograph counting could account for some of the differences with the sieving method, but also clast counts on x-radiographs may include low density “mud pellets” and diagenetic particles, that are either disaggregated or discarded in visual observations by the sieving method. Despite this caveat, in all of our studied sites there is consistency between sieve and

Prydz Bay deep-sea contourite drift deposit with IRD - ODP site 1165

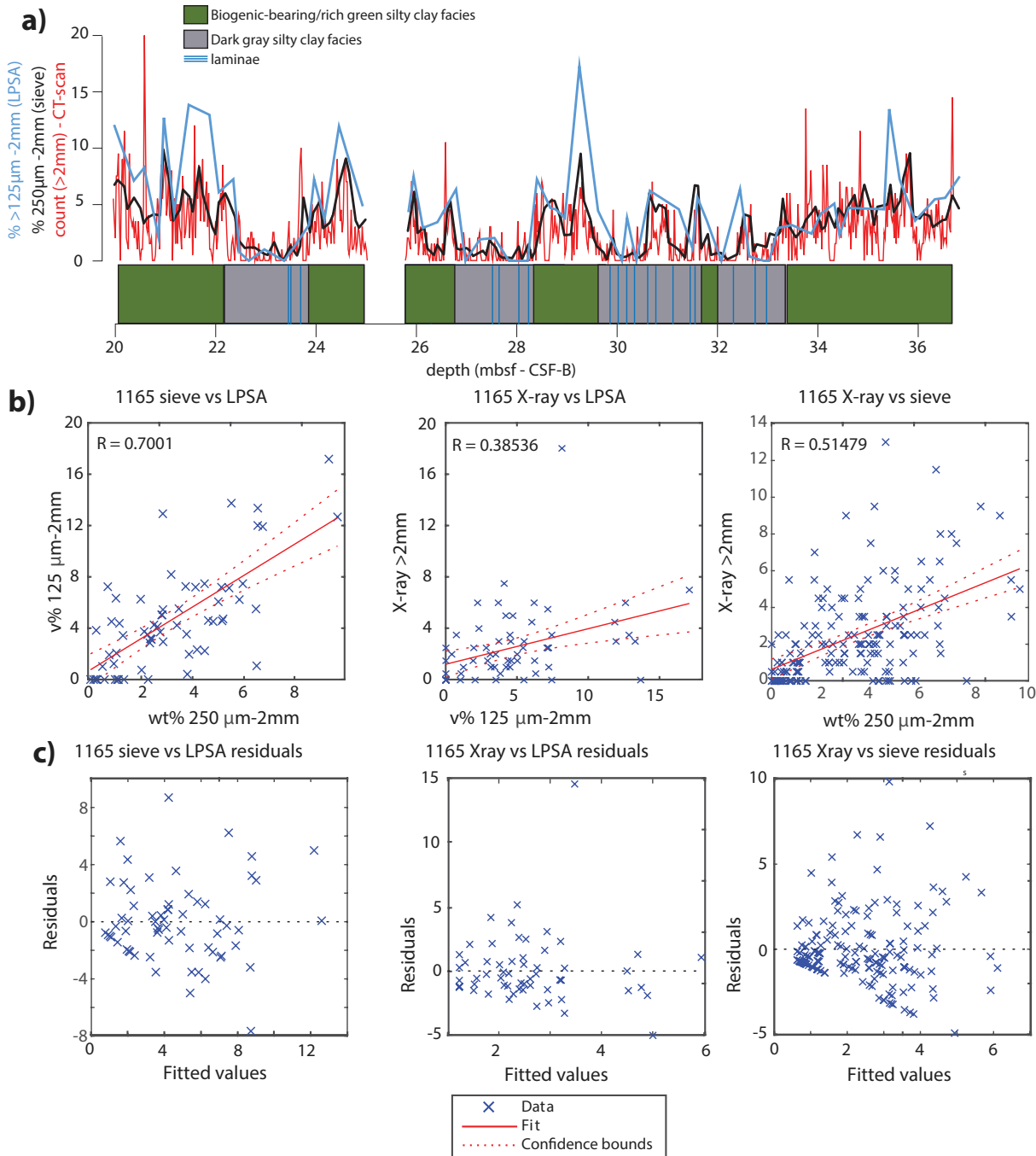


Figure 9. (a) Downcore comparison of measurements for coarse grain size fractions from sieve ($>250 \mu\text{m}$), LPSA methods ($>125 \mu\text{m}$ from Passchier, 2011) and x-radiograph (x-ray) methods at ODP Site 1165, a mixed turbidite levee and contourite drift deposit on the continental rise offshore from Prydz Bay (O'Brien et al., 2001); Lithological column is based on color reflectance data interpretations of lithofacies (Rebesco, 2003), observations of bioturbation and laminae occurrence in CT-scan photos, and are adjusted to the CSF-B depth-scale to correct for core expansion. (b) Cross plot of sieve-based measurements of $>250 \mu\text{m}$ weight percentages and LPSA $>125 \mu\text{m}$ percentages at ODP Site 1165, with linear regression model and 95% confidence bounds. (c) Plot of residuals versus fitted values from the linear regression model for plot in panel (b).

x-radiograph methods, but less consistency between x-radiograph and LPSA methods. This suggests the sieve and x-radiograph methods have a higher signal-to-noise ratio than the LPSA method when attempting to quantify a size fraction that could be interpreted as IRD, although site-specific aspects regarding IRD concentrations and statistical significance of the 250 μm –2 mm and >2 mm fraction should also be considered in any assessment of these size fractions representing IRD. Additionally, defining if these coarse fractions are indeed ice rafted is a separate, but equally important consideration, and can only really be assessed in tandem with visual examination of the coarse fraction (i.e., volcanic, eolian, and biogenic origins) alongside assessment of the full grain size frequency distributions via LPSA analysis.

In a continental margin setting there remains the possibility that any of the above methods could also record downslope processes, and the fine fraction and sedimentary descriptions/interpretation should be used to rule out mass flow and winnowing processes that could result in IRD being overestimated at any given core site. Geophysical datasets, such as seismic profiles and multibeam bathymetry are also useful tools to assess the broad-scale sedimentary processes that could potentially deliver or rework coarse-grained material to any given site, and whether such processes have to be considered at a finer resolution by the core sedimentology. While our study is not explicitly defending whether the particular grain size fractions we examine indeed represent IRD, the datasets we present provide indicators that 125 μm may not always be suitable as a lower cut-off size limit for IRD in all depositional settings on the Antarctic margin. Almost all of the sites we examine with LPSA measurement display grain size frequency distributions that contain well-sorted coarse silt to fine sand modes, with shoulders of these modes passing into the >125 μm fraction. These are likely to be due to either the presence of bottom currents transporting fine sands in the bed load (e.g., RS15-LC42 and RS15-LC48), or due to delivery of sands via turbidity currents (e.g., IODP Site U1361; Figure 8). The strong visual comparison of the results from ODP Site 1165, and lack of systematic biases in the cross plots, indicate the contourite drifts at that site may be suitable for assigning a lower cut-off limit of 125 μm (e.g., Passchier, 2011). However, a key advantage of the CT-scan dataset is that it provides a far higher resolution dataset than either the sieve or LPSA methods (Figure 9). Assessment of the full frequency distribution range would be a useful tool, alongside measures of sorting (cf. Passchier, 2011; McCave & Andrews, 2019), to verify whether the LPSA is indeed a reliable assessment of the IRD content, but also to provide improved confidence that post-depositional winnowing is not concentrating IRD.

5.2. IRD Mass Accumulation Rates Versus Lag Deposits

All of the above methods also need to consider winnowing processes that may act to concentrate IRD. The sorting parameter [spread of the sizes around the mean (Folk & Ward, 1957)] of the terrigenous component using LPSA analyses has been used as evidence that winnowing process have resulted in concentration of coarser grained particles (Passchier, 2011; Patterson et al., 2014). It is assumed that if a peak in the IRD MAR coincides with a well-sorted terrigenous sand fraction, then these peaks may be caused by winnowing of fine-grained material due to high-energy bottom currents. For this assumption to hold, a comparison of the source sediment and the resultant sediment deposit must be made in order to identify the sedimentary transport process (e.g., winnowing), and thus, it is not possible to identify the depositional environment from a single parameter derived from the grain-size frequency distribution. This problem is exaggerated in glaciated margin settings, where grain size populations are commonly multimodal. These modes result from a range of sediment delivery processes, via gravity/traction currents, glacimarine outwash, hemipelagic settling, and ice rafting. Therefore, winnowing of muds with minor sands/gravels could result in a sediment with a more even distribution of mud/sand and gravel and is therefore more poorly sorted than it was prior to winnowing.

Consequently, a more prudent approach to assess if the original IRD MAR is preserved in a stratigraphic section is to use a range of parameters determined from the grain-size frequency distribution, including mean grain size, skewness and sorting, alongside sedimentary structures of the deposit to assess for evidence of winnowing (McCave & Andrews, 2019; Rebesco et al., 2014). The presence of cross-laminae and scour features in silt and sandy silt beds in both RS15-LC42 and RS15-LC48 indicates that current velocities reached at least 23 cm s^{-1} that is required for movement of silt (McCave & Hall, 2006). However, while current-induced erosion has had some influence at both RS15 sites, sorting is consistently poor at both sites and shows no clear relationship to IRD content, suggesting that for most of the core there is no current influence on IRD content, but more careful attention is clearly warranted for specific intervals. We do not address this issue further in this paper, as the influence of bottom currents and distinguishing these from primary IRD deposition has been recently reviewed

for glacial settings in detail by McCave and Andrews (2019), who recommend running correlation coefficients of fine fraction sorting versus IRD to more rigorously define downcore changes in this relationship.

6. Determining IRD Mass Accumulation Rates: Implications of Using Different Methodologies

Raw IRD abundance fractions are a critical component of determining IRD MAR, but the grain size cut-off values for determining IRD differ between methods, and as a result, the absolute abundances of IRD MAR calculated will also vary, making intercomparisons between methods problematic. However, the differences between methods also have significant implications for the calculations used to determine IRD MAR. All IRD MAR calculation methods require determination of Dry Bulk Density (DBD) and Linear Sedimentation Rates (LSR), and these are effectively uniform between methods. DBD values are often measured in much lower resolution than the IRD sample spacings, and thus DBD values are required to be interpolated to the IRD sample spacing, usually using the nearest neighbor approach (e.g., Patterson et al., 2014; St. John & Krissek, 1999). This may not be appropriate in cores where there is large amount lithological variation; although regression-based methods of the low resolution DBD data to linescan datasets (GRAPE Density; XRF) and facies distribution in a core could also be used to improve resolution. Similarly, LSRs are also dependent on resolution of the age model, and this can result in large artifacts when determining MARs and is likely to be the largest influence on uncertainties in IRD MARs. For example, short duration magnetic reversals could amplify any sharp pulses in sedimentation that might otherwise be missed in longer duration polarity intervals, where the time averaging is longer and short phases with high sedimentation are muted by long periods with low background sedimentation rates. Consequently, caution should be exercised in interpretation of large pulses or baseline shifts of IRD MAR that coincide with paleomagnetic boundaries, as well as comparing IRD MAR curves between different sites that have age models of different resolution – as well as shifts in the quality of an age model down core. Again, a facies-based approach could help with identifying where sedimentation rates are likely to occur within polarity zones.

The above caveats exist for all determinations of MAR (including those of non-IRD variables), but the difference in methods in determining IRD MAR have some stand-alone considerations – in particular corrections for the presence of biogenic material. Consequently, we focus on the uncertainties in IRD MAR calculation that will result from using different methodological procedures. The sieve method captures the 250 µm–2 mm coarse sand percent and this can easily be visually checked for biogenic/diagenetic/volcanic ash content to determine the percent IRD within the 250 µm–2 mm fraction (St. John & Krissek, 1999).

Consequently, the following equation:

1. $\text{IRD MAR} = \text{IRD} \times \text{CS}_{250 \mu\text{m}-2 \text{ mm}} \times \text{DBD} \times \text{LSR}$

where the IRD MAR is in g/cm²/kyr, CS_{250 µm–2 mm} is the proportion of the 250 µm–2 mm grain-size fraction in respect to the bulk sediment (on a weight basis), DBD is in g/cm³, and LSR is the interval average LSR in cm/kyr. In this method IRD is visually estimated and corrected for (used as a decimal fractional value in the above equation). Thus, this is only a qualitative estimate of the weight percent, which is compounded further by the biogenic material such as diatoms or radiolarians having a significantly lower density (i.e., they are porous and hollow) than detrital or authigenic grains.

In the sieve-based method of Patterson et al. (2014), and our study, biogenic silica and foraminifera were chemically treated from the 250 µm to 2 mm sand fraction only, which removes the potentially qualitative aspect of counting biogenic particles as a volumetric component and converting these to a weight estimate (see methods). Subsequent to chemical treatment, each sample was visually reexamined under a binocular microscope to check for fresh volcanic ash, clay aggregates, and diagenetic minerals. These can either be visually corrected for, or a more conservative approach is to discard the samples. This allows for a simple modification of equation one.

2. $\text{IRD MAR} = \text{CS}_{\text{Terr}250 \mu\text{m}-2 \text{ mm}} \times \text{DBD} \times \text{LSR}$

where CS%_{Terr250 µm–2 mm} is the proportion of the 250 µm–2 mm grain size fraction weight in respect to the bulk sediment (on a weight basis), which is left after treatment to remove biogenic material.

To determine the %>125 µm using the LPSA method, the entire bulk sediment is treated with 10% HCl, 27% H₂O₂ and 1M NaOH solution to remove biogenic particles and organic matter prior to measurement. This is an important distinction from the sieve method particle size range that only removes biogenic material from the

>250 µm fraction. As NaOH treatment is suggested to have the potential to dissolve fine clays, an independent method for determining opal in the bulk sediment is often used. In this method, IRD MAR is calculated according to the methodology of Passchier (2011) with the following equation:

$$3. \text{IRD MAR} = \text{CS}_{125 \mu\text{m}-2 \text{ mm}} \times \text{TERR} \times \text{DBD} \times \text{LSR}$$

Aside from the lower cut-off of 125 µm to calculate CS, and that it is based on volume percentage, the TERR is the terrigenous fraction calculated by subtraction of the %CaCO₃ and %Biogenic silica from the bulk sediment fraction (i.e., the entire grain size distribution) as a weight percentage. The %CaCO₃ and %Biogenic silica datasets are commonly at lower resolutions than grain size measurements and require interpolation between values or use regression-based methods (Passchier, 2011), introducing their own uncertainties, which are not propagated into the above calculation. While such uncertainties will be consistent within a given methodology, the use of different methodological approaches make comparison of IRD MAR between sites problematic. Another key uncertainty in this method is the assumption that %CS_{125µm-2 mm} does not require correction for other non-IRD fraction. We discuss the possibility of other processes influencing this size fraction above, but volcanic ash, diagenetic minerals and other non-IRD particles could be present, and independent methods will be required to determine if these are present in a sediment population (Passchier et al., 2021). It could be argued this is also the case for x-radiograph based methods, although the 2 mm cut-off for defining an IRD grain means visual examination of the core face is likely to be sufficient for a trained operator to identify diagenetic grains and particles delivered by volcanic eruptive processes.

7. Conclusions

An assessment of the IRD content in several cores from the Antarctic margin was undertaken using the following three methodologies: (a) sieve analysis (250 µm–2 mm) providing IRD contents in weight percentage, (b) LPSA volume estimates of the 125 µm–2 mm fraction; and (c) visual counts of clasts exceeding 2 mm in size identified in x-radiographs. The sieve analysis and x-radiograph clast counts show a moderate-to-strong correlation. The LPSA analysis and x-radiograph clast counts also display good correlations in some settings, but are in general weaker. The lower correlation values between IRD content determined by LPSA and other methods in most of the studied sites, suggests the LPSA method is less precise and less accurate with respect to measuring its respective size fraction used to determine IRD. We suspect that the primary reason for this is the very small sample size (~0.15–0.9 g) that is required for the correct obscuration of the laser particle sizer for samples of these lithologies. A consequence of the small sample size is that the coarse “tail” of the grain size distribution of a poorly sorted sandy mud may potentially be represented by relatively few grains. Further complicating this method is that the lower cut-off of 125 µm may also sample material that is not ice rafted in origin (e.g., turbidite sands).

The higher correlation of sieve-based estimates and X-radiograph counts for IRD appears to be a less noisy representation of the IRD component than the LPSA >125 µm method in the samples we examined from Antarctic continental margin sediments. However, this does not rule out the use of LPSA data in defining an IRD population in a sample, indeed in some settings such as ODP Site 1165 it correlated well. For all methods, we argue that careful assessment of the various caveats regarding sample processing and analysis, and depositional processes need to be conducted. While we suggest LPSA is a noisier signal, x-radiograph and sieve methods also suffer from potential statistical significance issues in some settings.

Regardless of the method used, careful assessment of grain size frequency distributions and parameters, in combination with robust sedimentary descriptions of structures and visual examination of the coarse fraction must be used before a selected size fraction can be deemed as ice rafted. The exact size fraction used to define IRD will vary depending on depositional setting, and due diligence must be conducted in each study location. Assessment of sedimentary structures or grain size frequency data that indicate sediment winnowing or delivery of coarse material (e.g., fine sand and greater) by non-ice rafting should be mandatory before designating sand particles as IRD. In addition, although the use of a single statistical parameter to assess the influence of deep-water seabed erosion on continental margin sedimentary sequences may be valid in some situations, it should be used with caution in sediments with multimodal grain size populations—sediments that are pervasive in glaciated margins. Our study highlights the importance of assessing methodological impacts on IRD abundance within different depositional settings on the Antarctic margin, and provides guidance for glaciated margin sediments to assess if outsized particles in a grain size population are likely to be ice rafted in origin.

Data Availability Statement

All LPSA, sieve grain size, and x-radiograph count datasets for this research are available from McKay et al. (2020).

Acknowledgments

We thank the crews of R/V Araon for their support. New Zealand funding was provided by Royal Society Te Aparangi Marsden Fund (18-VUW-089) and the New Zealand Ministry of Business, Innovation and Employment through the Antarctic Science Platform (ANTA1801). This research was funded by the Korea Polar Research Institute (KOPRI) project PE22090. We thank the Integrated Ocean Drilling Program (IODP) and the Australia-New Zealand IODP Consortium (ANZIC). ANZIC is supported by the Australian Government through the Australian Research Council's LIEF funding scheme [LE0882854] and the Australian and New Zealand consortium of universities and government agencies. Open access publishing facilitated by Victoria University of Wellington, as part of the Wiley - Victoria University of Wellington agreement via the Council of Australian University Librarians.

References

- Amante, C., & Eakins, B. W. (2009).ETOPO1 Global Relief Model converted to PanMap layer format [Data set]. NOAA-National Geophysical Data Center. <https://doi.org/10.1594/PANGAEA.769615>
- Anderson, J. B. (1999). *Antarctic marine geology*. UK: Cambridge University Press.
- Andrews, J. (2000). Icebergs and iceberg rafted detritus (IRD) in the North Atlantic: Facts and assumptions. *Oceanography*, 13(3), 100–108. <https://doi.org/10.5670/oceanog.2000.19>
- Andrews, J. T., & Voelker, A. H. L. (2018). “Heinrich events” (& sediments): A history of terminology and recommendations for future usage. *Quaternary Science Reviews*, 187, 31–40. <https://doi.org/10.1016/j.quascirev.2018.03.017>
- Bassis, J. N., Petersen, S. V., & MacCathles, L. (2017). Heinrich events triggered by ocean forcing and modulated by isostatic adjustment. *Nature*, 542(7641), 332–334. <https://doi.org/10.1038/nature21069>
- Blott, S. J., & Pye, K. (2006). Particle size distribution analysis of sand-sized particles by laser diffraction: An experimental investigation of instrument sensitivity and the effects of particle shape. *Sedimentology*, 53(3), 671–685. <https://doi.org/10.1111/j.1365-3091.2006.00786.x>
- Bond, G., Heinrich, H., Broecker, W., Labeyrie, L., McManus, J., Andrews, J., et al. (1992). Evidence for massive discharges of icebergs into the North Atlantic ocean during the last glacial period. *Nature*, 360(6401), 245–249. <https://doi.org/10.1038/360245a0>
- Carroll, D., & Starkey, H. C. (1971). Reactivity of clay minerals with acids and alkalies. *Clays and Clay Minerals*, 19(5), 321333. <https://doi.org/10.1346/CCMN.1971.0190508>
- Carter, L., Neil, H. L., & Northcote, L. (2002). Late Quaternary ice-rafting events in the SW Pacific Ocean, off eastern New Zealand. *Marine Geology*, 191(1–2), 19–35. [https://doi.org/10.1016/S0025-3227\(02\)00509-1](https://doi.org/10.1016/S0025-3227(02)00509-1)
- Chewings, J. M., Atkins, C. B., Dunbar, G. B., & Golledge, N. R. (2014). Aeolian sediment transport and deposition in a modern high-latitude glacial marine environment. *Sedimentology*, 61(6), 1535–1557. <https://doi.org/10.1111/sed.12108>
- Clark, P. U., & Pisias, N. G. (2000). Interpreting iceberg deposits in the deep sea. *Science*, 290(5489), 51–52. <https://doi.org/10.1126/science.290.5489.51c>
- Conolly, J. R., & Ewing, M. (1965). Ice-rafted detritus as a climatic indicator in Antarctic deep-sea cores. *Science*, 150(3705), 1822–1824. <https://doi.org/10.1126/science.150.3705.1822>
- Cook, C. P., Hill, D. J., van de Flierdt, T., Williams, T., Hemming, S. R., Dolan, A. M., et al. (2014). Sea surface temperature control on the distribution of far-traveled Southern Ocean ice-rafted detritus during the Pliocene. *Paleoceanography*, 29(6), 2014PA002625. <https://doi.org/10.1002/2014PA002625>
- Cowan, E. A., Hillenbrand, C.-D., Hassler, L. E., & Ake, M. T. (2008). Coarse-grained terrigenous sediment deposition on continental rise drifts: A record of Plio-Pleistocene glaciation on the Antarctic Peninsula. *Palaeogeography, Palaeoclimatology, Palaeoecology*, 265(3), 275–291. <https://doi.org/10.1016/j.palaeo.2008.03.010>
- Cowan, E. A., Zellers, S. D., Müller, J., Walczak, M. H., Worthington, L. L., Caissie, B. E., et al. (2020). Sediment controls dynamic behavior of a Cordilleran Ice Stream at the last glacial maximum. *Nature Communications*, 11(1), 1826. <https://doi.org/10.1038/s41467-020-15579-0>
- Croudace, I. W., Rindby, A., & Rothwell, R. G. (2006). Itrax: Description and evaluation of a new multi-function X-radiograph core scanner. *Geological Society, London, Special Publications*, 267(1), 51–63. <https://doi.org/10.1144/GSL.SP.2006.267.01.04>
- DeConto, R., Pollard, D., & Harwood, D. (2007). Sea ice feedback and Cenozoic evolution of Antarctic climate and ice sheets. *Paleoceanography*, 22, PA3214. <https://doi.org/10.1029/2006PA001350>
- Depoorter, M. A., Bamber, J. L., Griggs, J. A., Lenaerts, J. T. M., Ligtenberg, S. R. M., van den Broeke, M. R., & Moholdt, G. (2013). Calving fluxes and basal melt rates of Antarctic ice shelves. *Nature*, 502, 89–92. <https://doi.org/10.1038/nature12567>
- Diekmann, B. (2007). Sedimentary patterns in the late Quaternary Southern Ocean. *Deep Sea Research Part II: Topical Studies in Oceanography*, 54(21), 2350–2366. <https://doi.org/10.1016/j.dsri.2007.07.025>
- Diekmann, B., Fütterer, D. K., Grobe, H., Hillenbrand, C. D., Kuhn, G., Michels, K., et al. (2003). Terrigenous sediment supply in the polar to temperate South Atlantic: Land-ocean links of environmental changes during the late quaternary. In G. Wefer, S. Multizzi, & V. Ratmeyer (Eds.), *The South Atlantic in the late Quaternary: Reconstruction of material budgets and current systems* (pp. 375–399). Berlin, Heidelberg: Springer. https://doi.org/10.1007/978-3-642-18917-3_18
- Donda, F., Brancolini, G., O'Brien, P. E., De Santis, L., & Escutia, C. (2007). Sedimentary processes in the Wilkes Land margin: A record of the Cenozoic East Antarctic Ice Sheet evolution. *Journal of the Geological Society*, 164(1), 243–256. <https://doi.org/10.1144/0016-76492004-159>
- Dowdeswell, J. A., Elverhøi, A., Andrews, J. T., & Hebbeln, D. (1999). Asynchronous deposition of ice-rafted layers in the Nordic seas and north Atlantic Ocean. *Nature*, 400(6742), 348–351. <https://doi.org/10.1038/22510>
- Ehrmann, W. U., & Grobe, H. (1991). Cyclic sedimentation at sites 745 and 746. *Proceedings of the Ocean Program, Scientific Results, ODP, Kerguelen Plateau-Prydz Bay*, 119, 225–237.
- Escutia, C., Brinkhuis, H., & Klaus, A. (2011). *Proceedings of the Ocean Drilling Program, Expedition 318, Wilkes Land Glacial History*. Retrieved from <http://publications.iodp.org/proceedings/318/318title.html>
- Escutia, C., Warnke, D., Acton, G. D., Barcena, A., Burkle, L., Canals, M., & Fazee, C. S. (2003). Sediment distribution and sedimentary processes across the Antarctic Wilkes Land margin during the Quaternary. *Deep Sea Research Part II: Topical Studies in Oceanography*, 50(8–9), 1481–1508. [https://doi.org/10.1016/S0967-0645\(03\)00073-0](https://doi.org/10.1016/S0967-0645(03)00073-0)
- Evans, J., & Pudsey, C. J. (2002). Sedimentation associated with Antarctic Peninsula ice shelves: Implications for palaeoenvironmental reconstructions of glaciomarine sediments. *Journal of the Geological Society*, 159(3), 233–237. <https://doi.org/10.1144/0016-764901-125>
- Flückiger, J., Knutti, R., & White, J. W. C. (2006). Oceanic processes as potential trigger and amplifying mechanisms for Heinrich events. *Paleoceanography*, 21(2). <https://doi.org/10.1029/2005PA001204>
- Folk, R. L., & Ward, W. C. (1957). Brazos River bar [Texas]; a study in the significance of grain size parameters. *Journal of Sedimentary Research*, 27(1), 3–26. <https://doi.org/10.1306/74D70646-2B21-11D7-8648000102C1865D>
- Gilbert, R. (1990). Rafting in glaciomarine environments. *Geological Society, London, Special Publications*, 53(1), 105–120. <https://doi.org/10.1144/GSL.SP.1990.053.01.06>

- Golledge, N. R., Menzel, L., Carter, L., Fogwill, C. J., England, M. H., Cortese, G., & Levy, R. H. (2014). Antarctic contribution to meltwater pulse 1A from reduced Southern Ocean overturning. *Nature Communications*, 5. <https://doi.org/10.1038/ncomms6107>
- Grobe, H. (1987). A simple method for the determination of ice rafted debris in sediment cores. *Polarforschung*, 57, 123–126. <https://doi.org/10.1080/1046171x.1987.12034306>
- Grobe, H., & Mackensen, A. (1992). Late Quaternary climatic cycles as recorded in sediments from the Antarctic continental margin. *Antarctic Research Series - American Geophysical Union*, 56, 349–376.
- Hansen, M. A., Passchier, S., Khim, B.-K., Song, B., & Williams, T. (2015). Threshold behavior of a marine-based sector of the East Antarctic Ice Sheet in response to early Pliocene ocean warming. *Paleoceanography*, 30(6), 2014PA002704. <https://doi.org/10.1002/2014PA002704>
- Heinrich, H. (1988). Origin and consequences of cyclic ice rafting in the Northeast Atlantic Ocean during the past 130,000 years. *Quaternary Research*, 29(2), 142–152. [https://doi.org/10.1016/0033-5894\(88\)90057-9](https://doi.org/10.1016/0033-5894(88)90057-9)
- Hemming, S. R. (2004). Heinrich events: Massive late Pleistocene detritus layers of the North Atlantic and their global climate imprint. *Reviews of Geophysics*, 42(1). <https://doi.org/10.1029/2003RG000128>
- Hepp, D. A., Mörz, T., & Grützner, J. (2006). Pliocene glacial cyclicity in a deep-sea sediment drift (Antarctic Peninsula Pacific Margin). *Paleogeography, Palaeoclimatology, Palaeoecology*, 231(1–2), 181–198. <https://doi.org/10.1016/j.palaeo.2005.07.030>
- Hillenbrand, C.-D., & Fütterer, D. (2001). Neogene to Quaternary deposition of opal on the continental rise west of the Antarctic Peninsula, ODP Leg 178, Sites 1095, 1096, and 1101. In P. F. Barker, A. Camerlenghi, G. D. Acton, & A. T. S. Ramsay (Eds.), *Proceedings of the Ocean Drilling Program Science Results* (Vol. 1, p. 178). <https://doi.org/10.2973/odp.proc.sr.178.215.2001>
- Hillenbrand, C.-D., Fütterer, D., Grobe, H., & Frederichs, T. (2002). No evidence for a Pleistocene collapse of the West Antarctic Ice Sheet from continental margin sediments recovered in the Amundsen Sea. *Geo-Marine Letters*, 22(2), 51–59. <https://doi.org/10.1007/s00367-002-0097-7>
- Hillenbrand, C.-D., Kuhn, G., & Frederichs, T. (2009). Record of a Mid-Pleistocene depositional anomaly in West Antarctic continental margin sediments: An indicator for ice-sheet collapse? *Quaternary Science Reviews*, 28(13–14), 1147–1159. <https://doi.org/10.1016/j.quascirev.2008.12.010>
- Hulbe, C. L., MacAyeal, D. R., Denton, G. H., Kleman, J., & Lowell, T. V. (2004). Catastrophic ice shelf breakup as the source of Heinrich event icebergs. *Paleoceanography*, 19(1). <https://doi.org/10.1029/2003PA000890>
- Jansen, E., Fronval, T., Rack, F., & Channell, J. E. T. (2000). Pliocene-Pleistocene ice rafting history and cyclicity in the Nordic Seas during the last 3.5 Myr. *Paleoceanography*, 15(6), 709–721. <https://doi.org/10.1029/1999PA000435>
- Jung, J., Park, Y., Lee, K., Hong, J.-P., Lee, J., Yoo, K., et al. (2019). Clay Mineralogical characteristics and origin of sediments deposited during the Pleistocene in the Ross Sea, Antarctica. *Journal of the Mineralogical Society of Korea*, 32(3), 163–172. <https://doi.org/10.9727/jmsk.2019.32.3.163>
- Kanfoush, S. L., Hodell, D. A., Charles, C. D., Guilderson, T. P., Mortyn, P. G., & Ninnemann, U. S. (2000). Millennial-scale instability of the Antarctic ice sheet during the last glaciation. *Science*, 288(5472), 1815–1819. <https://doi.org/10.1126/science.288.5472.1815>
- Kanfoush, S. L., Hodell, D. A., Charles, C. D., Janecek, T. R., & Rack, F. R. (2002). Comparison of ice-raftered debris and physical properties in ODP Site 1094 (South Atlantic) with the Vostok ice core over the last four climatic cycles. *Paleogeography, Palaeoclimatology, Palaeoecology*, 182(3), 329–349. [https://doi.org/10.1016/S0031-0182\(01\)00502-8](https://doi.org/10.1016/S0031-0182(01)00502-8)
- King, M. V., Gales, J. A., Laberg, J. S., McKay, R. M., De Santis, L., Kulhanek, D. K., et al. (2022). Pleistocene depositional environments and links to cryosphere-ocean interactions on the eastern Ross Sea continental slope, Antarctica (IODP Hole U1525A). *Marine Geology*, 443, 106674. <https://doi.org/10.1016/j.margeo.2021.106674>
- Kowalenko, C. G., & Babu, D. (2013). Inherent factors limiting the use of laser diffraction for determining particle size distributions of soil and related samples. *Geoderma*, 193–194, 22–28. <https://doi.org/10.1016/j.geoderma.2012.09.006>
- Lamy, F., Arz, H. W., Kilian, R., Lange, C. B., Lembeck-Jene, L., Wengler, M., et al. (2015). Glacial reduction and millennial-scale variations in Drake Passage throughflow. *Proceedings of the National Academy of Sciences*, 112(44), 13496–13501. <https://doi.org/10.1073/pnas.1509203112>
- Lewis, D. W., & McConchie, D. (1994). *Practical sedimentology* (2nd Ed.). New York: Chapman and Hall. Retrieved from <https://trove.nla.gov.au/version/44779937>
- Li, G., & Piper, D. J. W. (2015). The influence of meltwater on the Labrador current in Heinrich event 1 and the Younger Dryas. *Quaternary Science Reviews*, 107, 129–137. <https://doi.org/10.1016/j.quascirev.2014.10.021>
- Liu, Y., Moore, J. C., Cheng, X., Gladstone, R. M., Bassis, J. N., Liu, H., et al. (2015). Ocean-driven thinning enhances iceberg calving and retreat of Antarctic ice shelves. *Proceedings of the National Academy of Sciences*, 112(11), 3263–3268. <https://doi.org/10.1073/pnas.1415137112>
- Lucchi, R. G., Rebasco, M., Camerlenghi, A., Busetti, M., Tomadin, L., Villa, G., et al. (2002). Mid-late Pleistocene glacimarine sedimentary processes of a high-latitude, deep-sea sediment drift (Antarctic Peninsula Pacific margin). *Marine Geology*, 189(3–4), 343–370. [https://doi.org/10.1016/S0025-3227\(02\)00470-X](https://doi.org/10.1016/S0025-3227(02)00470-X)
- Marcott, S. A., Clark, P. U., Padman, L., Klinkhammer, G. P., Springer, S. R., Liu, Z., et al. (2011). Ice-shelf collapse from subsurface warming as a trigger for Heinrich events. *Proceedings of the National Academy of Sciences*, 108(33), 13415–13419. <https://doi.org/10.1073/pnas.1104772108>
- McCave, I. N., & Andrews, J. T. (2019). Distinguishing current effects in sediments delivered to the ocean by ice. I. Principles, methods and examples. *Quaternary Science Reviews*, 212, 92–107. <https://doi.org/10.1016/j.quascirev.2019.03.031>
- McCave, I. N., & Hall, I. R. (2006). Size sorting in marine muds: Processes, pitfalls, and prospects for paleoflow-speed proxies. *Geochemistry, Geophysics, Geosystems*, 7(10). <https://doi.org/10.1029/2006GC001284>
- McKay, R. M., Albion, O. B., Dunbar, G. B., Lee, J. I., Lee, M. K., Yoo, K.-C., et al. (2020). Ice rafted debris proxies for sediment cores RS15-LC42, RS15-LC48, IODP Site 318-U1361 and ODP Site 118-1165. [Dataset]. PANGAEA. <https://doi.org/10.1594/PANGAEA.920653dataset>
- McKay, R. M., De Santis, L., Kulhanek, D. K., & IODP Expedition 374 Science Team. (2019). *Proceedings of the International Ocean Discovery Program*, 374. <https://doi.org/10.14379/iodp.proc.374.2019>
- Müller, P. J., & Schneider, R. (1993). An automated leaching method for the determination of opal in sediments and particulate matter. *Deep Sea Research Part I: Oceanographic Research Papers*, 40(3), 425–444. [https://doi.org/10.1016/0967-0637\(93\)90140-X](https://doi.org/10.1016/0967-0637(93)90140-X)
- Murphy, L., Warnke, D. A., Andersson, C., Channell, J., & Stoner, J. (2002). History of ice rafting at South Atlantic ODP site 177-1092 during the Gauss and late Gilbert Chrons. *Paleogeography, Palaeoclimatology, Palaeoecology*, 182(3–4), 183–196. [https://doi.org/10.1016/S0031-0182\(01\)00495-3](https://doi.org/10.1016/S0031-0182(01)00495-3)
- Nielsen, S. H. H., Hodell, D. A., Kamenov, G., Guilderson, T., & Perfitt, M. R. (2007). Origin and significance of ice-rafted detritus in the Atlantic sector of the Southern Ocean. *Geochemistry, Geophysics, Geosystems*, 8(12), Q12005. <https://doi.org/10.1029/2007GC001618>
- O'Brien, P. E., Cooper, A. K., Richter, C., & the Shipboard Scientific Party. (2001). *Proceedings of the Ocean Drilling Program, Initial Reports* (Vol. 188). College Station, TX (Ocean Drilling Program). <https://doi.org/10.2973/odp.proc.ir.188.2001>

- Ó Cofaigh, C., & Dowdeswell, J. A. (2001). Laminated sediments in glacimarine environments: Diagnostic criteria for their interpretation. *Quaternary Science Reviews*, 20(13), 1411–1436. [https://doi.org/10.1016/S0277-3791\(00\)00177-3](https://doi.org/10.1016/S0277-3791(00)00177-3)
- Ó Cofaigh, C., Dowdeswell, J. A., & Pudsey, C. J. (2001). Late Quaternary iceberg rafting along the Antarctic Peninsula continental rise and in the Weddell and Scotia seas. *Quaternary Research*, 56(3), 308–321. <https://doi.org/10.1006/qres.2001.2267>
- Ohneiser, C., Yoo, K.-C., Albott, O. B., Cortese, G., Riesselman, C., Lee, J. I., et al. (2019). Magneto-biostratigraphic age models for Pleistocene sedimentary records from the Ross Sea. *Global and Planetary Change*, 176, 36–49. <https://doi.org/10.1016/j.gloplacha.2019.02.013>
- Passchier, S. (2011). Linkages between East Antarctic ice sheet extent and Southern Ocean temperatures based on a Pliocene high-resolution record of ice-rafter debris off Prydz Bay, East Antarctica. *Paleoceanography*, 26, 13 PP. <https://doi.org/10.1029/2010PA002061>
- Passchier, S., Hansen, M. A., & Rosenberg, J. (2021). Quartz grain microtextures illuminate Pliocene periglacial sand fluxes on the Antarctic continental margin. *The Depositional Record*, 7(3), 564–581. <https://doi.org/10.1002/dep2.157>
- Patterson, M. O., McKay, R., Naish, T., Escutia, C., Jimenez-Espejo, F. J., Raymo, M. E., et al. (2014). Orbital forcing of the east Antarctic ice sheet during the Pliocene and early Pleistocene. *Nature Geoscience*, 7(11), 841–847. <https://doi.org/10.1038/ngeo2273>
- Powell, R., & Domack, G. W. (2002). 12-modern glaciomarine environments. In J. Menzies (Ed.), *Modern and past glacial environments* (pp. 361–389). Oxford: Butterworth-Heinemann. <https://doi.org/10.1016/B978-075064226-2/50015-5>
- Pudsey, C. J. (2002). Neogene record of Antarctic Peninsula glaciation in continental rise sediments: ODP Leg 178, site 1095. *Proceedings of the Ocean Drilling Program: Scientific Results*, 178, 1–25.
- Rackow, T., Wesche, C., Timmermann, R., Hellmer, H. H., Juricke, S., & Jung, T. (2017). A simulation of small to giant Antarctic iceberg evolution: Differential impact on climatology estimates. *Journal of Geophysical Research: Oceans*, 122, 3170–3190. <https://doi.org/10.1002/2016JC012513>
- Rawle, A. F. (2015). Representative sampling – another Cinderella of particle size analysis. *Procedia Engineering*, 102, 1707–1713. <https://doi.org/10.1016/j.proeng.2015.01.306>
- Rebesco, M. (2003). Data report: Numerical evaluation of diffuse spectral reflectance data and correlation with core photos, ODP Site 1165, Wild Drift, Cooperation Sea, Antarctica. In A. K. Cooper, P. E. O'Brien, & C. Richter (Eds.), *Proceedings of the Ocean Drilling Program: Scientific Results* (Vol. 188). <https://doi.org/10.2973/odp.proc.sr.188.006.2003>
- Rebesco, M., Hernández-Molina, F. J., Van Rooij, D., & Wählén, A. (2014). Contourites and associated sediments controlled by deep-water circulation processes: State-of-the-art and future considerations. *Marine Geology*, 352, 111–154. <https://doi.org/10.1016/j.margeo.2014.03.011>
- Ruddiman, W. F. (1977). Late Quaternary deposition of ice-rafter sand in the subpolar North Atlantic (lat 40° to 65°N). *GSA Bulletin*, 88(12), 1813–1827. [https://doi.org/10.1130/0016-7606\(1977\)88<1813:LQDOIS>2.0.CO;2](https://doi.org/10.1130/0016-7606(1977)88<1813:LQDOIS>2.0.CO;2)
- Ryves, D. B., Juggins, S., Fritz, S. C., & Battarbee, R. W. (2001). Experimental diatom dissolution and the quantification of microfossil preservation in sediments. *Palaeogeography, Palaeoclimatology, Palaeoecology*, 172(1), 99–113. [https://doi.org/10.1016/S0031-0182\(01\)00273-5](https://doi.org/10.1016/S0031-0182(01)00273-5)
- St John, K., & Krissek, L. A. (1999). Regional patterns of Pleistocene ice-raftered debris flux in the North Pacific. *Paleoceanography*, 14(5), 653–662. <https://doi.org/10.1029/1999PA900030>
- St John, K., Passchier, S., Tantillo, B., Darby, D., & Kearns, L. (2015). Microfeatures of modern sea-ice-raftered sediment and implications for paleo-sea-ice reconstructions. *Annals of Glaciology*, 56(69), 83–93. <https://doi.org/10.3189/2015AoG69A586>
- Starr, A., Hall, I. R., Barker, S., Rackow, T., Zhang, X., Hemming, S. R., et al. (2021). Antarctic icebergs reorganize ocean circulation during Pleistocene glacials. *Nature*, 589(7841), 236–241. <https://doi.org/10.1038/s41586-020-03094-7>
- Strachan, L. J., Bostock, H. C., Barnes, P. M., Neil, H. L., & Gosling, M. (2016). Non-cohesive silt turbidity current flow processes; insights from proximal sandy-silt and silty-sand turbidites, Fiordland, New Zealand. *Sedimentary Geology*, 342, 118–132. <https://doi.org/10.1016/j.sedgeo.2016.06.017>
- Stuart, K. M., & Long, D. G. (2011). Tracking large tabular icebergs using the SeaWinds Ku-band microwave scatterometer. *Deep Sea Research Part II: Topical Studies in Oceanography*, 58(11), 1285–1300. <https://doi.org/10.1016/j.dsr2.2010.11.004>
- Talarico, F. M., McKay, R. M., Powell, R. D., Sandroni, S., & Naish, T. (2012). Late Cenozoic oscillations of Antarctic ice sheets revealed by provenance of basement clasts and grain detrital modes in ANDRILL core AND-1B. *Global and Planetary Change*, 96(97), 23–40. <https://doi.org/10.1016/j.gloplacha.2009.12.002>
- Teitler, L., Warnke, D. A., Venz, K. A., Hodell, D. A., Becquey, S., Gersonde, R., & Teitler, W. (2010). Determination of Antarctic Ice Sheet stability over the last ~500 ka through a study of iceberg-raftered debris. *Paleoceanography*, 25(1). <https://doi.org/10.1029/2008PA001691>
- Tournadre, J., Bouthier, N., Girard-Ardhuin, F., & Rémy, F. (2016). Antarctic icebergs distributions 1992–2014. *Journal of Geophysical Research: Oceans*, 121(1), 327–349. <https://doi.org/10.1002/2015JC011178>
- Tulaczyk, S., Kamb, B., Scherer, R. P., & Engelhardt, H. F. (1998). Sedimentary processes at the base of a West Antarctic ice stream; constraints from textural and compositional properties of subglacial debris. *Journal of Sedimentary Research*, 68(3), 487–496.
- Warner, N. R., & Domack, E. W. (2002). Millennial- to decadal-scale paleoenvironmental change during the Holocene in the Palmer Deep, Antarctica, as recorded by particle size analysis. *Paleoceanography*, 17, PAL-5. <https://doi.org/10.1029/2000PA000602>
- Weber, M. E., Clark, P. U., Kuhn, G., Timmermann, A., Sprenk, D., Gladstone, R., et al. (2014). Millennial-scale variability in Antarctic ice-sheet discharge during the last deglaciation. *Nature*, 510(7503), 134–138. <https://doi.org/10.1038/nature13397>
- Williams, T., & Handwerger, D. (2005). A high-resolution record of early Miocene Antarctic glacial history from ODP Site 1165, Prydz Bay. *Paleoceanography*, 20(2), PA2017. <https://doi.org/10.1029/2004PA001067>
- Williams, T., van de Flierdt, T., Hemming, S. R., Chung, E., Roy, M., & Goldstein, S. L. (2010). Evidence for iceberg armadas from East Antarctica in the Southern Ocean during the late Miocene and early Pliocene. *Earth and Planetary Science Letters*, 290(3–4), 351–361. <https://doi.org/10.1016/j.epsl.2009.12.031>
- Wilson, D. J., Bertram, R. A., Needham, E. F., Flierdtvan de, T., Welsh, K. J., McKay, R. M., et al. (2018). Ice loss from the East Antarctic Ice Sheet during late Pleistocene interglacials. *Nature*, 561, 383–386. <https://doi.org/10.1038/s41586-018-0501-8>